Ma *et al. Biochar* (2026) 8:103
https://doi.org/10.1007/s42773-026-00622-y

Biochar

ORIGINAL RESEARCH Open Access

Interactive effects of straw and biochar alter humic acid composition and component associations

Rui Ma[1], Xiaodong Zheng[1], Yifeng Zhang[2], Xiang Li[1], Lan Wei[1], Lianxi Huang[1], Wenke Zhang[1], Qimei Lin[1], Zhenqing Shi[3*] and Zhongzhen Liu[1*]

Abstract

Humic acid (HA), a key component of soil humic substances, plays a crucial role in soil fertility and ecological functioning. To investigate HA structural heterogeneity under contrasting organic inputs, a soil incubation experiment was conducted with straw and biochar applied individually and in combination. HA was characterized using complementary techniques, including elemental analysis, electron paramagnetic resonance (EPR), 3D excitation-emission matrix fluorescence spectroscopy (3D-EEM), transmission electron microscopy (TEM), solid-state ^{13}C nuclear magnetic resonance (^{13}C-NMR), and Fourier transform ion cyclotron resonance mass spectrometry (FT-ICR-MS). Biochar application preferentially enriched aromatic and structurally condensed components of HA, whereas straw inputs increased the abundance of oxygenated moieties associated with molecular biodegradability. Strikingly, their combined application enhanced HA radical concentration and chemical activity while favoring a shift in aromatic composition toward less highly condensed aromatic structures, resulting in HA molecular assemblages that combine features commonly associated with higher chemical reactivity and increased structural persistence. These findings suggest that soil HA formation under co-application is characterized by a reactivity-stability coupling, whereby labile, oxygen rich components are reorganized within aromatic and structurally persistent molecular frameworks, as revealed by complementary spectroscopic and molecular network analyses. This study provides new strategies and theoretical foundations for optimizing soil organic matter stability and fertility.

Highlights

- Interactions between straw and biochar break the trade-off between reactivity and persistence, reshaping key properties of humic matter.
- Understanding humic acid through its molecular network organization reveals effects beyond those explained by single chemical indicators.
- Straw-biochar interactions assemble reactive and persistent components into an integrated humic architecture.

Keywords Biochar, Straw, Humic acid, Molecular structure, Reactivity-stability coupling

---

*Correspondence:
Zhenqing Shi
zqshi@scut.edu.cn
Zhongzhen Liu
lzzgz2001@163.com
Full list of author information is available at the end of the article

© The Author(s) 2026. **Open Access** This article is licensed under a Creative Commons Attribution 4.0 International License, which permits use, sharing, adaptation, distribution and reproduction in any medium or format, as long as you give appropriate credit to the original author(s) and the source, provide a link to the Creative Commons licence, and indicate if changes were made. The images or other third party material in this article are included in the article's Creative Commons licence, unless indicated otherwise in a credit line to the material. If material is not included in the article's Creative Commons licence and your intended use is not permitted by statutory regulation or exceeds the permitted use, you will need to obtain permission directly from the copyright holder. To view a copy of this licence, visit http://creativecommons.org/licenses/by/4.0/.

Springer

Graphical Abstract

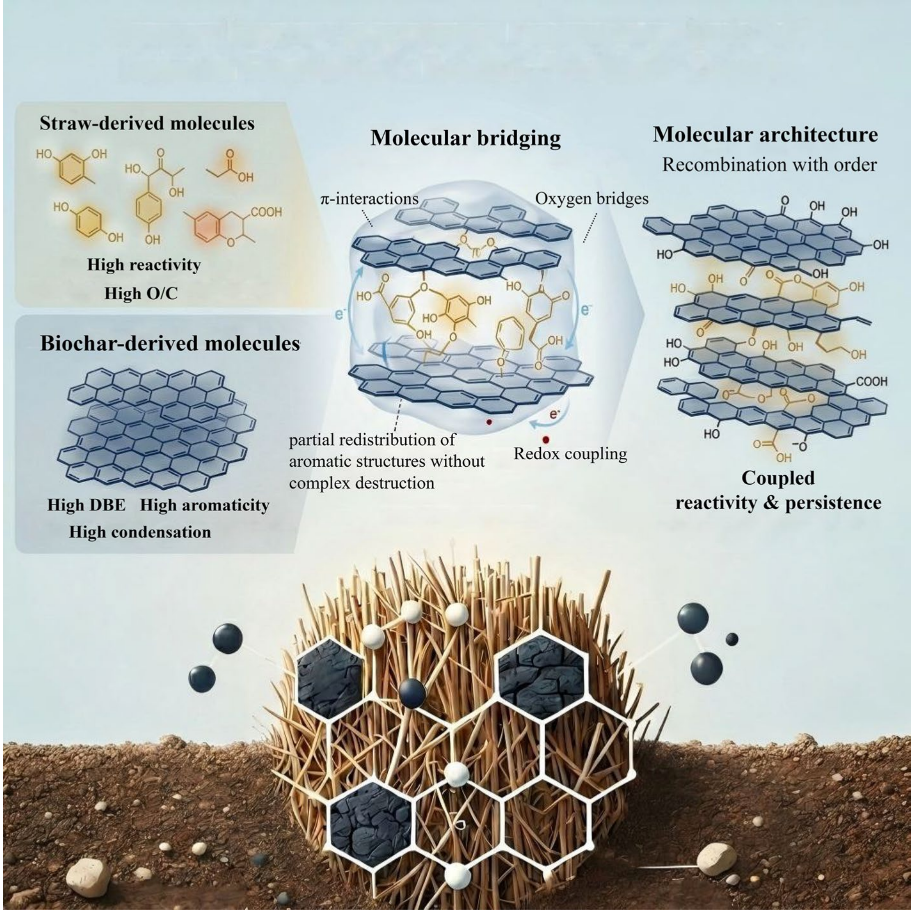

1 Introduction

Soil organic matter (SOM) is a central regulator of soil fertility, ecosystem functioning, and terrestrial carbon cycling. The traditional view of SOM considers humic substances, and particularly humic acid (HA), as a relatively persistent fraction that plays a critical role in nutrient retention, soil structure, and long-term carbon stabilization (Hayes and Clapp 2001; Helal et al. 2011; de Aguiar et al. 2022; Dou et al. 2025). Although the conceptual nature and formation pathways of humic substances have been widely debated, accumulating evidence indicates that HA exhibits broadly consistent molecular characteristics across soils, supporting its relevance as a meaningful target for investigating SOM stabilization processes (Hayes and Clapp 2001; Helal et al. 2011; de Aguiar et al. 2022; Dou et al. 2025). In light of ongoing debates and the progressive refinement of SOM conceptual frameworks, humic substances (HS) are increasingly reconsidered as operational representations of soil organic matter along a continuum of transformation and stabilization, rather than as independent chemical entities (Luo et al. 2025). In this context, HS provide a practical framework for distinguishing SOM fractions with different levels of reactivity and stability and for describing them at a finer level of resolution. Their associations with nutrient retention and release, soil-water interface processes, and hydrophobic-hydrophilic interactions therefore remain functionally informative when interpreted within this updated conceptual context (Olk et al. 2019; De Nobili et al. 2020; Stancampiano et al. 2023; Zhang et al. 2023; Yang et al. 2024).

Straw return and biochar application are two widely used exogenous carbon-input practices for increasing SOM in cropland soils (Enebe et al. 2025; Fu et al. 2025; Zhang et al. 2025; Di Gerónimo et al. 2026), but each has limitations when applied alone. Straw provides abundant labile carbon, stimulates microbial activity, and promotes the formation of young, highly reactive soil organic matter. However, these products are relatively unstable and often result in high-carbon input but low-carbon retention. Rapid straw decomposition may also disturb pre-existing humic structures and is commonly associated with lower aromaticity and molecular features indicative of reduced persistence (Liang et al. 2023; Ying et al. 2024; Koyama et al. 2025; Tao and Liu 2025). In contrast, biochar is characterized by high aromaticity and greater structural persistence, which favor soil organic carbon retention and improvement of soil physicochemical properties (Lehmann et al. 2011; Liu et al. 2022a; He et al. 2025). While biochar can enhance the stability of HA, its direct transformation into humic substances is generally limited due to its intrinsic recalcitrance (Jindo et al. 2016; Zhang et al. 2022).

Straw and biochar represent two contrasting types of organic inputs, with the former characterized by higher chemical reactivity and the latter by greater structural persistence (Liu et al. 2020; Lei et al. 2024a). Their combined application has therefore been proposed as a means of balancing short-term nutrient supply with long-term carbon stabilization (Xie et al. 2025). Previous studies have shown that straw-biochar co-application can influence soil organic carbon accumulation, humification, microbial activity, and aggregate formation. However, most of this work has remained at the level of bulk indicators, such as SOC, humification indices, or conventional spectroscopic characteristics, and has not yet answered a key question: whether co-application alters the relative abundance and molecular network features of reactive and stable components within HA.

To address this question, it is necessary to examine the molecular features of humic acid (HA). The relative abundance and combination of oxygen-containing and aromatic structures in HA can influence its susceptibility to decomposition, its persistence in soil, and its roles in nutrient retention and redox related processes (Sutton and Sposito 2005; Ou et al. 2023; Stancampiano et al. 2023). Examining HA at the molecular level therefore helps determine whether the combined application of straw and biochar changes the relative characteristics of reactive and stable components, and in turn improves our understanding of its effects on soil organic carbon stability (Piccolo 2016; Fedotov et al. 2023).

Accordingly, this study asks whether the co-application of straw and biochar reorganizes the molecular structure of humic acid in a manner distinct from single application. Using a controlled incubation experiment, we compared HA formed under straw, biochar, and combined straw-biochar treatments. Humic acid was characterized using elemental analysis, EEM fluorescence, EPR, solid-state ^{13}C NMR, TEM, and FT-ICR-MS. These methods were chosen to capture changes in oxygen-rich reactive structures, aromatic and condensed carbon, and supramolecular arrangements. Observed differences across treatments provide insights into how the two organic inputs influence HA composition and structural features, and how these features may relate to soil organic matter stability.

2 Materials and methods

2.1 Soils and materials

Soil samples were collected from a field site in Guangzhou, Guangdong province, a representative agricultural area in Southern China. The soil represents a typical highly weathered agricultural soil from subtropical regions. The collected soil samples are categorized as Oxisol, displaying a silt dominated loam texture composed of 15.4% clay, 60.5% silt, and 24.1% sand fractions. Bulk soil samples were collected from the surface layer (0–20 cm) of the arable land, which was sieved to pass through a 2 mm mesh screen following the removal of visible plant residues. The main properties of the sampled soil are presented in Table 1.

The straw samples were collected from Zhongluotan Demonstration Base for Agriculture, Guangdong Academy of Agricultural Sciences in Southern China. The straw was dried at 60 ℃, ground and passed through a 0.25 mm sieve, and stored in dry conditions prior to the experiment.

Portions of the straw were pyrolyzed at 450 ℃ in a programmed muffle furnace for 1 h to obtain biochar that was passed through a 0.25 mm sieve. Detailed physicochemical properties of biochar, and straw samples are shown in Tables S1.

2.2 Laboratory incubation experiment and analysis

Portions of the bulk soil (50 g oven dried mass per replicate, $n = 3$ independent replicates) were thoroughly mixed with either straw powder (PL), biochar (BL), or their co-application (BPL). Soil without application served as control (CK). In PL, the straw application rate was calculated based on a full return scenario corresponding to an annual maize straw yield of 12,000 kg ha^{-1}. In the present incubation system, based on the measured physicochemical properties of the straw used in this study, this rate corresponded to an exogenous organic carbon input of 2.91 g C kg^{-1} soil. Equal C amounts were applied in the BL, with 50% biochar C and 50% straw C in the BPL. All treatments were incubated in parallel under identical conditions in the dark at 25 ± 2 °C for 180 days. Soil moisture was initially adjusted to 60% of water holding capacity (WHC) and maintained during incubation by periodic weighing and replenishment with distilled water. To minimize evaporative loss, each soil sample was placed

Table 1 Basic properties of soil

Soil properties	pH	SOC (g kg^{-1})	DOC (mg kg^{-1})	DON (mg kg^{-1})	NH_4^+ (mg kg^{-1})	NO_3^- (mg kg^{-1})	TN (g kg^{-1})	Clay (%)	Silt (%)	Sand (%)
	5.81	18.1	76.3	74.5	4.01	23.7	1.71	15.4	60.5	24.1

into flat tubes (40 mm diameter, 120 mm height) and incubated in a sealed 1 L wide mouth jar containing a vial with 10 mL distilled water. During incubation, flat tubes were periodically weighed every week, and distilled water was added directly to the soil when necessary to restore the target moisture content. Soil pH was not artificially adjusted to a common value across treatments, because pH change was considered part of the treatment effect induced by straw and/or biochar addition. After the cultivation was completed, destructive sampling of soil samples was conducted and HA extraction and analysis were carried out.

To reduce confounding variability and facilitate mechanistic interpretation, this study intentionally employed one single soil type and standardized incubation conditions. This design allowed treatment-induced molecular differences in humic acid to be resolved with high analytical resolution. The 180-day incubation period does not represent the endpoint of humification but serves as a single time point for comparative analysis, capturing the cumulative transformation results. Previous studies have shown that, under typical soil conditions, approximately 50–70% of the degradable fraction of straw is decomposed by microorganisms within 3–6 months, with some lignin components breaking down more slowly. The molecular composition and structural characteristics of HA at this time point comprehensively reflect the cumulative effect of the three stages of decomposition in the early stage, transformation and recombination in the middle stage, and relative stabilization in the late stage, which is conducive to the analysis of more comprehensive molecular heterogeneity and transformation relationship.

2.3 Soil HA extraction and purification

Humic acid was extracted and purified following the International Humic Substances Society procedure, which was described in detail by Swift (1996). Briefly, 20 g air-dried soil was acidified to a pH of 1–2 with 1 M HCl solution. After centrifugation, the liquid phase was discarded. Following that, samples were extracted with a 0.1 M NaOH solution and left to stand overnight. The HA supernatant was soaked in a mixture of HF and HCl solutions overnight in order to minimize the ash content. The resulting HA was electrodialyzed, then concentrated by rotary evaporation before being freeze-dried to remove any remaining water.

2.4 Structural characterization and molecular composition analysis

To examine changes in humic acid (HA) across complementary structural levels, multiple analytical methods were combined rather than relying on a single technique. These methods were selected to capture bulk elemental characteristics, carbon functional group distribution, fluorescent components, radical-active sites, molecular formula composition, and nanoscale aggregate morphology of HA.

Elemental composition (C, H, N, and O) was determined to assess the overall chemical composition of HA and to derive elemental ratios related to its structural characteristics. 3D excitation emission matrixfluorescence spectroscopy (3D-EEM) was used to characterize humic-like fluorescent components and conjugated oxygen-containing aromatic moieties, with commonly used fluorescence indices calculated to indicate relative humification and microbial contribution Electron paramagnetic resonance (EPR) spectroscopy was applied to detect environmentally persistent free radicals and to characterize redox-active radical environments associated with oxygen-containing and conjugated aromatic structures in HA. Solid-state ^{13}C nuclear magnetic resonance (^{13}C NMR) spectroscopy was used to quantify the distribution of major carbon structural groups, including alkyl C, O-alkyl C, aromatic C, and carboxyl/carbonyl C, in order to compare changes in oxygenated and aromatic carbon fractions among treatments. Transmission electron microscopy (TEM) was used to observe the nanoscale morphology and aggregate features of HA, providing structural information at the supramolecular level.

High-resolution FT-ICR-MS was used to resolve molecular formula composition and infer treatment-related differences in oxidation degree, unsaturation, and aromaticity based on van Krevelen analysis, Kendrick mass defect analysis, and derived indices including DBE, AImod, NOSC, and aromaticity equivalent.

Together, these methods were used to assess whether straw, biochar, and their combined application produced different patterns in oxygen-rich reactive features, aromatic and condensed features, and nanoscale organization of HA. Detailed analytical procedures and calculation methods are provided in the Supporting Information.

It is necessary to clarify that FT-ICR-MS mainly detects the soluble and ionizable fraction of HA, and large or highly aggregated components may be underrepresented. However, this method is highly reproducible and suitable for comparing relative molecular composition among treatments (Goranov et al. 2022). Therefore, the FT-ICR-MS results are interpreted as relative differences within the detectable HA fraction rather than as a complete representation of all HA components. Related structural characterizations are interpreted as reflecting the relative behavior and transformation tendency of extracted HA under standardized analytical conditions, rather than the in situ structure of HA in soil. Details of structural characterization, molecular composition analysis, and FT-ICR-MS data processing are provided in the **Supplementary Information**.

2.5 Network construction and analysis

A molecular transformation network was constructed from FT-ICR-MS assigned molecular formulas based on exact mass differences corresponding to common biogeochemical reactions. Nodes represent individual molecular formulas, and edges represent potential transformations inferred from predefined reaction rules. Network analyses were performed to characterize molecular connectivity, structural importance, and higher order organization within the transformation network (Kitson et al. 2021; Traquete et al. 2022; Cai et al. 2023). Node level importance was first evaluated using PageRank and complementary centrality measures to capture both global influence and local connectivity patterns. In this chemical context, PageRank can be intuitively understood as a measure of how centrally a molecular formula is embedded within the inferred transformation network: molecules connected to many other well-connected molecules receive higher scores and can therefore be regarded as occupying more influential positions in the potential transformation space of HA.

In addition to overall centrality, reaction type distributions were quantified at both the network and community levels to examine how different transformation processes were organized across network modules (Brin and Page 1998; Page et al. 1999a; Kitson et al. 2021). As part of the network construction and validation procedure, mass difference matching errors were evaluated for all inferred transformations by comparing observed product masses with theoretical masses derived from predefined reaction Δm values. Errors were tightly centered around zero, reflecting the strict mass matching tolerance applied during network construction. Community detection was conducted on the undirected network to identify reaction modules. For each module, internal reaction type compositions were analyzed to assess the degree of transformation specificity within communities (Freeman 1978; Bonacich 1987; Page et al. 1999b; Brandes 2001). To facilitate interpretation of dominant transformation structures, high confidence subnetworks enriched in structurally important nodes were extracted. Weighted centrality metrics were applied to integrate network topology, signal intensity, and reaction plausibility, enabling the identification of a core reaction subnetwork. For consistency across treatment networks, FT-ICR-MS signal intensities were normalized to unit sum within each treatment dataset prior to analysis. Standard PageRank was calculated from network topology, whereas normalized intensities were used consistently across all treatments in intensity-related analyses, including PageRank-intensity correlations and weighted PageRank-based core subnetwork and backbone extraction. Within this core, backbone transformation chains were inferred to represent the most prominent and continuous transformation routes in the network. Detailed descriptions of reaction type analysis, weighted centrality calculations, and highly connected transformation chains identification procedures are provided in the **Supplementary Information**.

All network analyses were performed using Python, primarily relying on the NetworkX, NumPy, SciPy, and Matplotlib libraries (Hagberg et al. 2007). Custom scripts were developed to ensure reproducibility and are available upon reasonable request.

3 Results and discussion

3.1 Visual analysis of HA

TEM analyses of HA from each treatment identified distinct nanoscale morphologies (Fig. 1d): dot-like particles, lamellar structures (4–6 nm in diameter), and elongated fibers with bundled arrangements. EDS analyses correlated higher C concentrations with increased contrast, indicating that the observed grayscale variation primarily reflected internal C distribution rather than staining artifacts (Fig. S1). Elongated chain-like and linear fibers appear to represent the same structural motif viewed from different orientations on the membrane, consistent with prior electron microscopy observations that HA can appear as shape variable aggregates rather than single uniform “macromolecules” (Fedotov et al. 2023). High-C polymeric materials occurred only in PL. In BPL treatments, these polymers progressively disintegrated into smear-like morphologies consisting of particles and fiber bundles. This apparent shift in observed morphology is difficult to reconcile with a strictly covalent polymer growth mechanism alone; instead, it is more consistent with the now widely discussed view that humic substances are dynamic associations of relatively small components stabilized by non-covalent forces (e.g., hydrogen bonding and π-π stacking), whose apparent size and morphology can reorganize upon environmental/chemical perturbations (Piccolo 2001; Sutton and Sposito 2005; Baveye and Wander 2019).

At the 10 nm scale, striped lattice-like structures with average spacings of 0.268–0.388 nm were observed (Fig. 1d), occurring preferentially in C rich regions. Such ordered spacings suggest the presence of ordered lattice like features or layered organic assemblies, analogous to the “ordered subdomains within supramolecular HA assemblies” reported in recent TEM-based fractionation work on HA (Trubetskaya et al. 2023, 2024, 2025). Under organic applications, stripe spacing increased, indicating

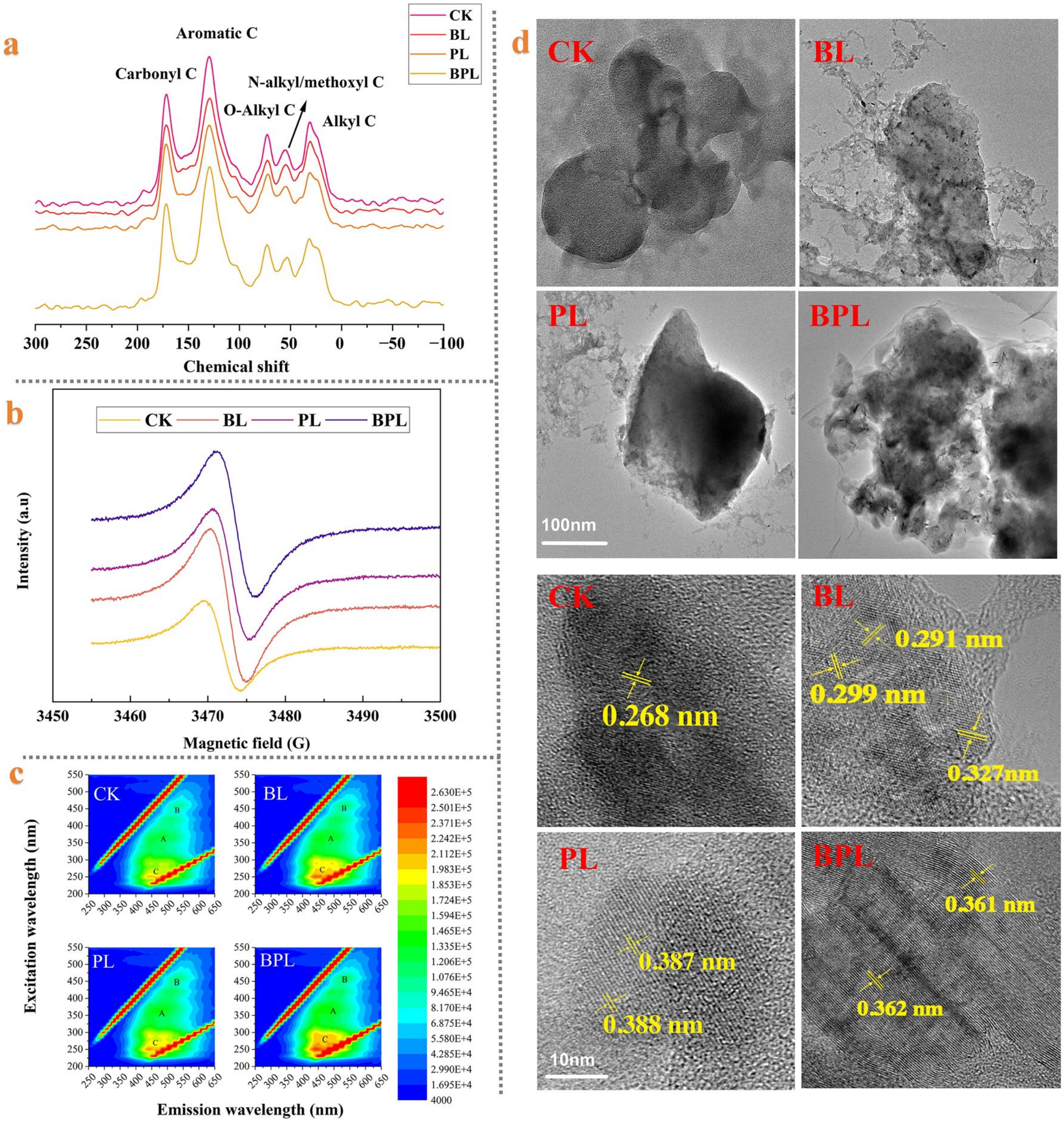

Fig. 1 **a** ^{13}C nuclear magnetic resonance spectra, **b** EPFR spectrum, **c** the 3D fluorescence spectrum and **d** the TEM images of humic acid under different treatments

a loosening and increasing irregularity of HA molecular organization, which may alter accessibility/reactivity by weakening packing constraints. Importantly, the magnitude of expansion differed across applications (smallest in BL and largest in PL), implying that biochar derived aromatic domains tend to maintain tighter packing/organization than straw derived oxygenated components, an interpretation aligned with the "supramolecular humification" framework where the balance between hydrophobic association and H bonding governs aggregate compactness and emergent functionality (Piccolo 2001; Sutton and Sposito 2005).

3.2 Elements and functional groups

The elemental composition captures bulk structural shifts in HA (Table 2). Compared to CK, all organic applications reduced C, H, and N contents and increased O content. Abiotic oxidation and microbial decomposition preferentially removed C- and H-rich aliphatic moieties, released CO_2 and H_2O, and partially mineralized N-containing components, and resulted in the relative

Table 2 Elemental composition of soil HA samples under different treatments

Treatments	N [%]	C [%]	H [%]	O [%]	H/C (mol)	O/C (mol)	C/N (mol)	O/H (mol)
CK	4.455	46.841	4.674	43.504	1.197	0.697	12.267	0.582
BL	4.39	46.693	4.345	44.053	1.117	0.708	12.409	0.634
PL	4.353	45.187	4.235	45.82	1.125	0.761	12.111	0.676
BPL	4.366	45.609	4.253	45.498	1.119	0.748	12.187	0.669

enrichment of O-containing groups in the residual HA (Schmidt et al. 2011b; Lehmann and Kleber 2015). BL produced the lowest H/C ratio,, placing HA in a more aromatically condensed state (Schmidt et al. 2011b; Wiedner et al. 2013), while PL induced the largest increase in O/C, characteristic of stronger oxidative processing of plant derived inputs (Wiedner et al. 2013); BPL retained both tendencies: showing H/C values closer to BL and O/C values approaching PL. Condensed and oxidized features therefore co-occurred within the same HA molecule rather than separating into mutually exclusive pathways. This integration likely resulted from biochar's surface area and active groups adsorbing straw-derived intermediates and interacting with soluble degradation products (low molecular weight acids, alcohols) via covalent, hydrogen, and van der Waals forces (Wang et al. 2016; Premalatha et al. 2023; Lei et al. 2024b; Enebe et al. 2025), together with straw-stimulated microbial activity and biochar-provided habitats that accelerated degradation and humus reassembly, generating HA with both condensation and oxidation features (Liu et al. 2022b; Jia et al. 2023). Among them, biochar functioned as a stabilizing aromatic matrix that retained straw-associated oxygen-rich reactive intermediates within its pores and on aromatic surfaces. These intermediates were then further incorporated into HA through adsorption, π-π interactions, quinone-phenolic coupling, and condensation reactions. The relatively persistent components specifically involved in this process mainly included condensed aromatic structures, biochar derived aromatic frameworks/domains, and quinone-/phenolic-containing aromatic moieties, which served as stable matrices for the incorporation and stabilization of straw-associated labile components. Consequently, all treatments increased O/H and enhanced polarity, with PL producing the most hydrophilic HA, BL the least polar, and BPL intermediate but closer to PL, indicating that straw-biochar interactions yield HA combining molecular features associated with BL derived structural condensation and PL derived oxidative reactivity (Schmidt et al. 2011b; Wiedner et al. 2013).

EPFR spectroscopy revealed distinct environmentally persistent free radicals ($g = 2.0029–2.0044$) within HA frameworks (Fig. 1b), confirming the widespread presence of organic radicals across all treatments (Table 3). Biochar application (BL) generated exclusively carbon centered aromatic radicals ($g = 2.0029$), a signal commonly associated with highly conjugated aromatic structures and metal-facilitated electron transfer that stabilize unpaired electrons through π-electron delocalization (Odinga et al. 2020; Chen et al. 2024). Elevated pH and relatively low redox potential under BL conditions further suppressed oxygen-centered radical formation and favored the persistence of carbon centered radicals via π-conjugated stabilization, consistent with previous interpretations of biochar derived EPFR behavior (Jia et al. 2018; Ruan et al. 2019; Liu et al. 2024; Li et al. 2025a). In contrast, straw application (PL) and co-application (BPL) treatments exhibited oxygen-centered radicals ($g > 2.0040$), typically attributed to oxygenated functional groups (e.g., hydroxyl, carboxyl, quinone) and redox-active intermediates such as peroxides and semiquinones derived from plant residues (Shi et al. 2020; Bi et al. 2022). Under BPL conditions, the porous structure

Table 3 EFPR and the relative intensity of fluorescence spectra of soil HA samples under different treatments

Treatment	G value	ΔH	EPFR spins g^{-1}	Fluorophore A SFI	Fluorophore B SFI	Fluorophore C SFI	FI	BIX	HIX
CK	2.0034	5.002	7.77×10^{7}	72.4	103.2	157.7	0.974	0.366	19.138
BL	2.0029	4.802	1.26×10^{8}	88.1	106.8	184.9	0.99	0.367	20.527
PL	2.00436	4.602	1.26×10^{8}	85.1	107.7	163.1	1.006	0.371	18.582
BPL	2.00423	5.603	1.29×10^{8}	83.9	109.1	184.9	1.051	0.377	17.72

of biochar may favor the retention of straw derived reactive intermediates within HA assemblages. In addition, π-π interactions between biochar associated aromatic domains and oxygen-centered radicals are consistent with enhanced radical abundance and persistence. Taken together, the co-occurrence of these radical signals suggests that labile substrates involved in radical generation may be incorporated into biochar stabilized molecular matrices, rather than remaining transient or being rapidly quenched (Qin et al. 2018; Guo et al. 2023; Yi et al. 2025).

Linewidths (ΔH = 4.6–5.6 G) narrowed under BL and PL, indicating simplified radical environments and reduced magnetic heterogeneity, whereas BPL exhibited broader linewidths, consistent with donor–acceptor coupling between biochar associated quinones and straw derived phenolics that generates spatially heterogeneous radical populations with altered magnetic properties (Wan et al. 2020; Rashid et al. 2022; Xie et al. 2024; Du et al. 2025; Liu et al. 2025). Carbon normalized EPFR concentrations ($(7.77–12.26) \times 10^7$ spins g^{-1} C) increased markedly in BL and PL, reflecting enhanced radical formation and reduced inter radical interactions, while BPL showed intermediate levels, integrating radical generation and stabilization mechanisms of both substrates.

In the EEM fluorescence spectra of HA (Fig. 1c), three characteristic peaks were identified, A (330–370/500–550 nm), B (450–465/515–535 nm), and C (255–270/490–526 nm), all of which were enhanced under organic applications (Table 3). Peak C is commonly associated with phenolic and quinone moieties exhibiting higher degrees of condensation, whereas peak B reflects polymerized aromatic macromolecules such as lignin or flavonoid like structures, and peaks A and C together represent composite humic like fluorescence components (Ateia et al. 2017; Liu et al. 2021).

Biochar application(BL) produced the largest increases in peaks A and C, placing HA in a more strongly conjugated, high-molecular-weight aromatic state, whereas straw application(PL) produced higher B peak fluorescence intensity, reflecting the direct incorporation of lignin and flavonoid derived components from plant residues (Wang et al. 2014; Cheng et al. 2024; Ying et al. 2024; Cui et al. 2025). BPL showed the smallest increase in peak A but matched BL in peak C intensity and also showed a pronounced redshift and the highest B peak intensity. Even under lower straw input, HA retained strong aromatic condensation and conjugation while incorporating straw-derived secondary metabolites. Biochar derived aromatic frameworks and redox-active sites can facilitate electron transfer and condensation reactions, thereby offsetting lower straw input and sustaining conjugated HA formation (Meng et al. 2023).

Fluorescence indices further supported this interpretation. All FI < 1.4 confirmed predominantly exogenous HA origins; FI still rose after organic application, with the smallest increase under BL and the largest under BPL, straw addition shifted HA toward a stronger microbial imprint, and the shift was strongest under BPL (Chin et al. 1994; Cory and McKnight 2005). BIX exhibited trends parallel to FI, reflecting greater proportions of newly formed, autochthonous HA in PL and BPL relative to BL (Liu et al. 2020). In contrast, HIX displayed an opposing pattern, increasing only under BL while decreasing under PL and further under BPL, indicating that although biochar applications promoted humification and aromaticity, straw applications, particularly when coupled with biochar favored the accumulation of more active HA. Together with the EPFR results, we found that HA formed under co-application retains high conjugation and redox activity despite weaker humification signatures, allowing reactivity and persistence to coexist within the same system.

Across all treatments, the ^{13}C NMR spectra of HA (Fig. 1a) displayed aromatic C was the dominant fraction (45.22–53.10%), followed by O-alkyl C, carbonyl C, and alkyl C (Table 4). Compared with CK, carbonyl, O-alkyl, and aliphatic C increased under all exogenous carbon treatment (BPL > PL > BL > CK), whereas aromatic C increased only under BL but declined under PL and BPL (BL > CK > PL > BPL). Biochar intrinsically enriched in condensed aromatic structures, promoted the incorporation and preservation of aromatic C within HA, whereas straw application favored the accumulation of oxygen containing, non-aromatic components and the transformation of pre-existing aromatic structures, consistent

Table 4 Relative carbon distribution (%) of HA in solid state ^{13}C-NMR spectra extracted from soils managed

Treatment	Carbonyl C 160–230 ppm	Aromatic C 110–160 ppm	O-Alkyl C 50–110 ppm	Alkyl C 0–50 ppm	Aliphatic C 0–110 ppm	Aliphatic C/Aromatic C	Alkyl C/O-alkyl C	Hydrophobic C/Hydrophilic C
CK	15.24	51.10	12.04	16.59	28.63	0.56	1.38	2.48
BL	17.65	52.54	15.24	16.28	31.52	0.60	1.07	2.09
PL	19.89	46.54	21.34	14.72	36.06	0.77	0.69	1.49
BPL	21.62	45.22	32.93	14.08	47.01	1.04	0.43	1.09

with previous NMR based observations that labile plant inputs tend to dilute aromatic signatures while enhancing O-alkyl and carbonyl pools. Notably, these effects were further amplified under combined application (BPL), suggesting that straw derived reactive substrates accelerate molecular turnover while biochar associated aromatic frameworks constrain complete aromatic loss. Consistent with these compositional shifts, key structural ratios changed markedly. Aliphatic/aromatic C ratios increased under BL and PL, alkyl/alkoxy C ratios decreased, and hydrophobic/hydrophilic C ratios declined across treatments, with the strongest shifts observed in BPL. Such ratio changes are commonly interpreted as indicators of reduced molecular condensation and hydrophobic protection, alongside enhanced chemical accessibility (Liu et al. 2021; de Aguiar et al. 2022).

3.3 Characteristics of the molecular composition of HA in the treatment

Given the complex composition of HA molecules, traditional analytical techniques are insufficient to fully resolve treatment-induced differences. Therefore, we employed FT-ICR-MS to comprehensively characterize molecular changes in soil HA under different treatments. A total of 3133–3857 compounds were identified, primarily CHO (57–72%), followed by CHON (19–31%), CHOS (6–9%),

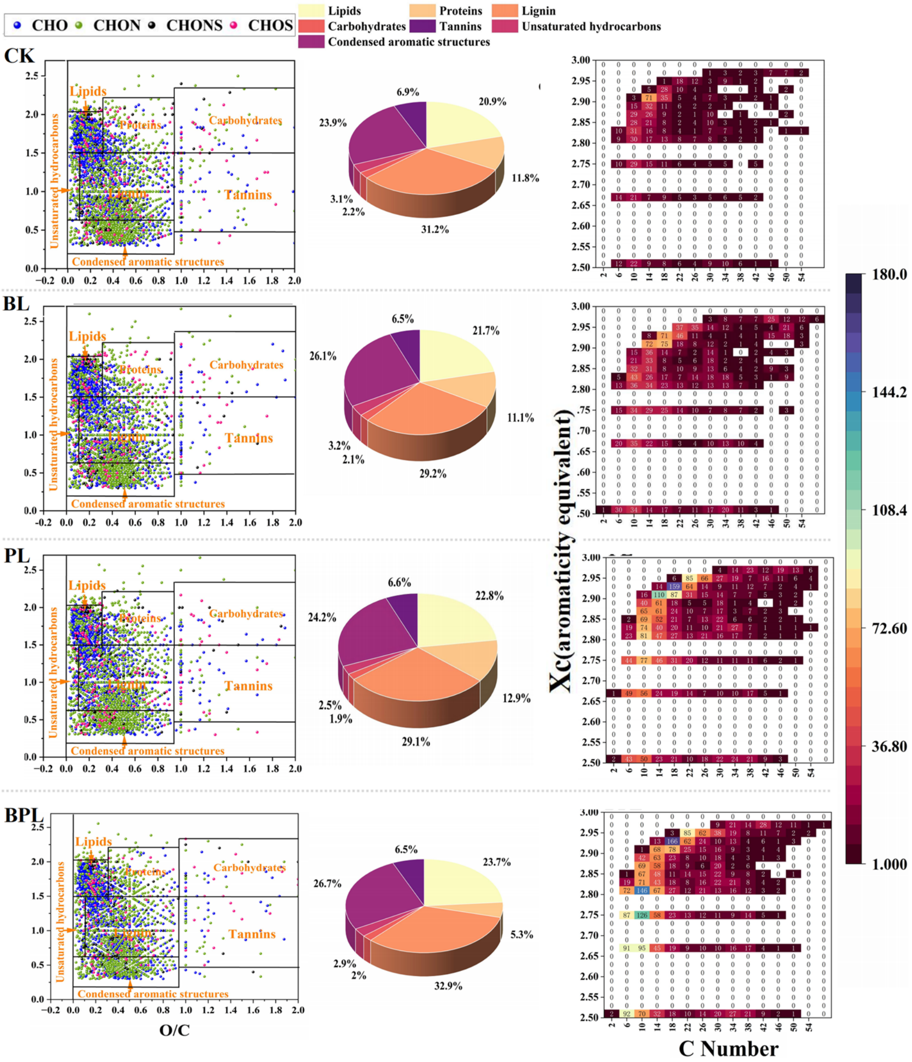

Fig. 2 Changes in molecular structure, the H/C and O/C distribution of HA molecules in van Krevelen diagrams the relative abundance of seven component groups of HA under different treatments. The plots of aromatic equivalent (Xc) as a function of carbon number for aromatic-free, aromatic, and condensed aromatic compounds of HA. The values of Xc ≥ 2.5000, Xc ≥ 2.71429, and Xc ≥ 2.80952 were considered to be the criteria for the presence of aromatic compounds and condensed aromatic structures

and CHONS (0.5–1%) (Fig. 2). Exogenous carbon inputs decreased the proportions of CHO, CHOS, and CHONS compounds, while increasing CHON. Relative to CK, BL reduced CHO (−0.2%), CHONS (−0.9%), and CHOS (−0.2%), whereas PL caused greater decreases. Notably, in the BPL treatment, CHONS and CHOS decreased, but both CHO and CHON increased, with the largest shifts among all treatments.

According to the van Krevelen diagram (Fig. 2), molecular distributions varied among treatments. To refine molecular classification, HA compounds were grouped into seven categories: lipids (H/C = 1.5–2.0, O/C = 0–0.3), proteins (H/C = 1.5–2.2, O/C = 0.3–0.67), lignin (H/C = 0.7–1.5, O/C = 0.1–0.67), carbohydrates (H/C = 1.5–2.4, O/C = 0.67–1.2), unsaturated hydrocarbons (H/C = 0.7–1.5, O/C = 0–0.1), condensed aromatics (H/C = 0.2–0.7, O/C = 0–0.67), and tannins (H/C = 0.5–1.5, O/C = 0.67–1.2) (Ohno et al. 2014). Relative abundances (Fig. 2) showed that lipids, lignin, and condensed aromatics together accounted for over 60% of HA across all treatments, followed by proteins (7–13%), tannins (6.4–6.9%), unsaturated hydrocarbons (2–4%), and carbohydrates (1–3%). Organic applications increased lipids, unsaturated hydrocarbons, and condensed aromatics. Compared with CK, BL contained the highest proportion of condensed aromatics (26.18%) but reduced proteins, lignin, and carbohydrates, whereas PL enriched lipids (23.3%), proteins (13.2%), and tannins (6.7%) while minimizing carbohydrates (1.94%). Under co-application (BPL), lipids, lignin, and tannins reached the highest proportions, and condensed aromatics were only 0.9% lower than in BL, indicating that straw-biochar interactions not only enhanced the abundance of chemically active structures but also maintained a high aromatic content, thereby strengthening molecular architectures commonly associated with reduced bioavailability. Mechanistically, straw mainly supplied oxygen-rich reactive precursors, whereas biochar contributed persistent aromatic domains. Under co-application, these biochar-associated aromatic frameworks retained and reorganized straw-associated labile intermediates, leading to their incorporation into HA through condensation and aromatic reassembly. Therefore, the interaction was specifically mediated by condensed aromatics, biochar-associated aromatic frameworks/domains, and quinone-/phenolic-containing aromatic moieties, rather than by a simple additive accumulation of two independent carbon inputs (Hertkorn et al. 2008; Kellerman et al. 2018; Chae et al. 2024).

Double bond equivalent (DBE) captures the abundance of double bonds and rings in organic molecules, higher values correspond to lower saturation and greater structural condensation (Zhou et al. 2023). DBE rises with molecular size, as unsaturated bonds and cyclic structures accumulate in larger molecules (Fig. 3b). Compared with BL and PL, BPL maintained higher DBE for compounds containing 20–40 carbon atoms and an even more pronounced increase at $C > 40$, indicating the formation of larger and more unsaturated molecular structures under co-application. The nominal oxidation state of carbon (NOSC) (Fig. 3c), tracks the redox state of organic matter, integrates information on both oxygen incorporation and molecular unsaturation, linking formula composition to potential biogeochemical reactivity (Han et al. 2025; Xiao et al. 2025). BPL also maintained higher NOSC (Fig. 3c), so straw-biochar interactions generated HA molecules that simultaneously possessed a greater degree of unsaturation and enriched oxygen containing functional groups. The co-occurrence of high DBE and high NOSC marks organic matter that remains chemically reactive while retaining substantial structural complexity, rather than representing purely labile or fully stabilized carbon pools. BPL pushes HA toward a more advanced transformation state, where enhanced oxygenation co-occurs with a high degree of retained aromatic condensation, enhancing chemical reactivity while simultaneously influencing longer-term stabilization pathways through molecular organization and redox buffering (Schmidt et al. 2011a; Kellerman et al. 2018).

According to the Aromaticity Index (AI) and H/C ratio, the van Krevelen diagram can be divided into four regions (Fig. 3a): aliphatic compounds ($2.0 \geq H/C \geq 1.5$), highly unsaturated and phenolic compounds ($AI \leq 0.50$ and $H/C < 1.5$), polyphenolic compounds ($0.66 \geq AI > 0.50$), and polycyclic aromatic compounds ($AI > 0.66$) (Kellerman et al. 2018). Because of the low ratio of CHONS to CHOS, AImod was calculated only for CHO and CHON species. Compared with CK, BL increased aliphatic and polycyclic aromatic fractions, PL reduced polycyclic aromatics but significantly enriched polyphenolics, while BPL yielded the highest proportion of aliphatics (35.5%) and intermediate levels of polycyclic aromatics and polyphenolics. Aromatic and condensed aromatic compounds with long alkyl chains were further characterized using the aromaticity equivalent Xc (Yassine et al. 2014), where $Xc \geq 2.5000$ and $Xc \geq 2.7143$ define aromatic and condensed aromatic compounds, respectively. Most HA molecules were identified as condensed aromatics, with fewer simple aromatics (Fig. 1). After application, both aromatic and condensed aromatic fractions increased, but BL mainly enriched condensed aromatics with C number of 20–30 ($Xc \geq 2.7143$), PL enhanced condensed aromatics with C number of 10–20, and BPL favored the formation of simpler aromatic compounds with lower aromaticity ($Xc \geq 2.5000$), the aromatic pool thus shifted

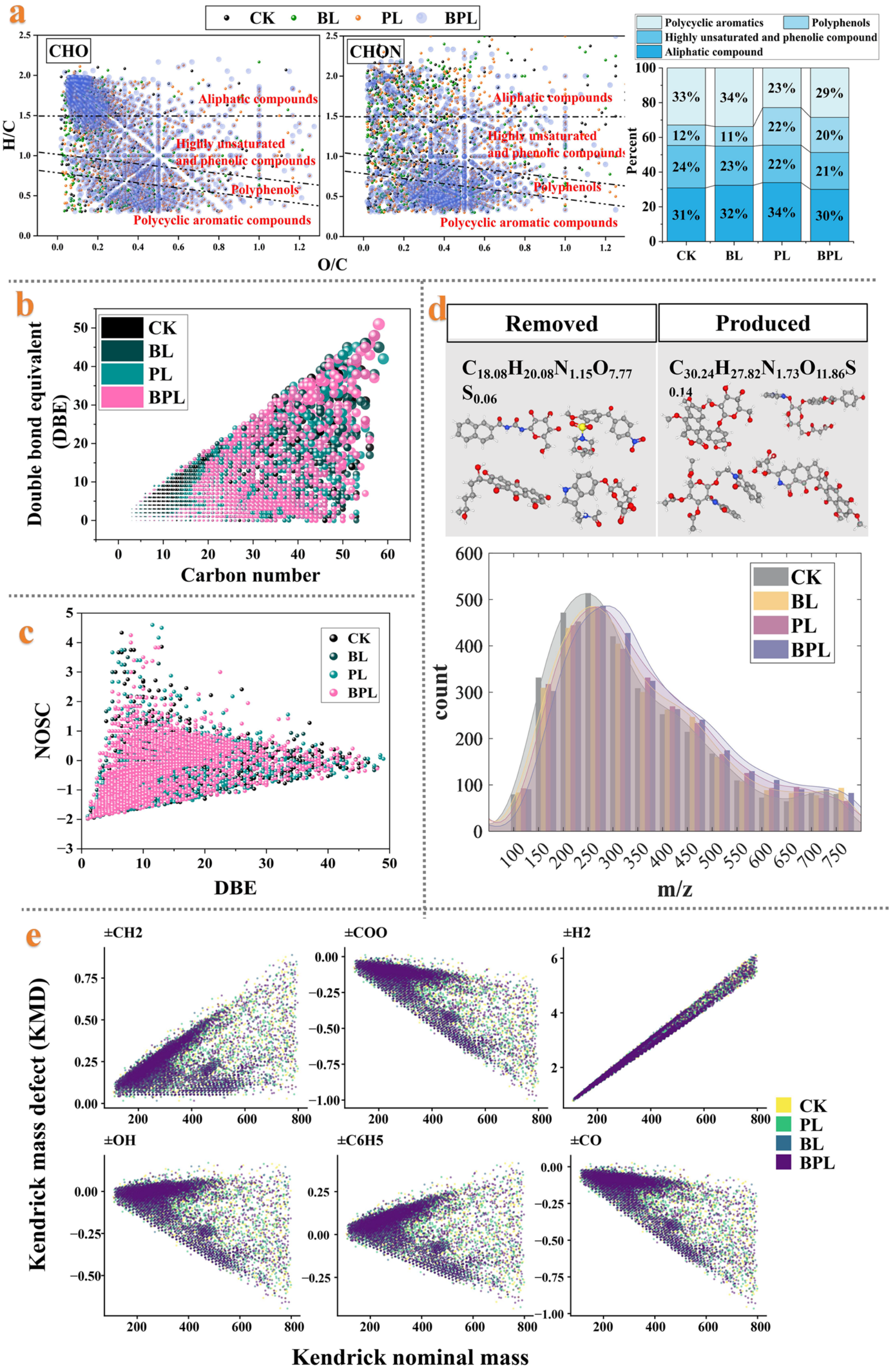

Fig. 3 **a** Based on elemental ratio diagrams derived from FT-ICR-MS analysis, molecular compositions were classified using threshold criteria of the aromaticity index (AI) to identify aliphatic, phenolic, polyphenolic, and polycyclic aromatic compounds, and to quantify their relative proportions, **b** Carbon number versus double bond equivalent (DBE) plot and **c** DBE vs. nominal oxidation state(NOSC) of carbon plots of HA molecules. **d** Kernel density plots of removed and produced HA structural components as a function of m/z, as well as **e** the Kendrick mass defect analysis of HA molecule for different treatments. BPL exhibited a broader redistribution pattern across low to intermediate KNM regions

from highly condensed structures toward less condensed aromatic molecules..

At different structural levels, the lower aromatic C detected by ^{13}C NMR under BPL corresponded to a redistribution and loosening of highly condensed aromatic domains at the supramolecular level. FT-ICR-MS, by contrast, captured the concurrent enrichment of simpler aromatic molecules with lower aromaticity equivalents. Co-application did not reduce aromaticity itself, but redistributed aromatic structures between highly condensed domains and less condensed molecular forms within HA.

Kendrick mass defect (KMD) analysis was applied to further investigate compound transformation and elimination during humification (Fig. 3e and Fig. S2). Based on KMD theory, organic molecules with identical KMD values are homologous and differ only in molecular weight, where Δm corresponds to integer multiples of selected functional group masses. Six functional groups were examined $\pm CH_2$ (methylation/demethylation), $\pm COO$ (carboxylation/decarboxylation), $\pm H_2$ (hydrogenation/dehydrogenation), $\pm OH$ (hydroxylation/dehydroxylation), $\pm C_6H_5$ (aromatication/dearomatication), and $\pm CO$ (carbonylation/decarbonylation) (Hughey et al. 2001). Among them, BL primarily removed CH_2, COO, and C_6H_5 groups at high Kendrick nominal mass, while promoting methylation, carboxylation, and aromatication in lower mass HA molecules. In contrast, PL removed H_2, OH, and CO at higher mass, while enhancing hydrogenation, hydroxylation, and carbonylation in lighter fractions. Under co-application (BPL), these processes converged: high mass compounds were cleaved into lower mass homologs, while methylation, hydrogenation, carboxylation, hydroxylation, aromatication, and carbonylation were simultaneously enhanced in low mass fractions. This dual effect not only eliminated excessively aged HA molecules but also increased the structural diversity of younger HA, consistent with the observed decrease in aromaticity and increase in unsaturation (Figs. 1, 3).

Comparison of KMD density distributions among treatments reveals clear, reaction-type-dependent contrasts across Kendrick nominal mass (KNM) domains (Fig. 4). Comparisons between single applications showed that PL was characterized by relative enrichment of oxygen related and hydrogenation associated homologous series ($\pm OH, \pm CO, \pm COO$, and $\pm H_2$) predominantly in low to intermediate KNM ranges (< 300–400), whereas BL exhibited higher densities of alkyl and aromatic related homologs ($\pm CH_2$ and $\pm C_6H_5$) concentrated in higher KNM domains (> 400). Relative to PL, co-application (BPL) consistently reduced relative representation of low KNM oxygenated and hydrogenation related structures, accompanied by redistribution toward intermediate KNM regions involving alkylated and aromatic associated series. In contrast, compared with BL, a pronounced reduction of high KNM alkyl and aromatic dominance under BPL, together with enhanced densities of multiple functional group homologs in low to intermediate KNM ranges. Across all six reaction types, BPL simultaneously attenuates the low mass, oxygen rich enrichment characteristic of PL, and the high mass, condensed aromatic and alkyl accumulation characteristic of BL, resulting in a broader redistribution of molecular populations across KNM space rather than amplification of a single transformation direction.

We conducted a detailed comparison of HA molecules formed under different treatments. In CK, HA exhibited a normal m/z distribution centered around 250, with an average molecular formula of $C_{18.08}H_{20.08}N_{1.15}O_{7.77}S_{0.06}$. After organic applications, distributions shifted toward higher m/z values: approximately 280 under BL and PL, and 300 under BPL, with the latter showing the most pronounced shift and an average formula of $C_{30.24}H_{27.82}N_{1.73}O_{11.86}S_{0.14}$ (Fig. 3d). PubChem based structural inference indicated that carbon-based unit addition promoted polymerization, condensation, and addition reactions, with BPL producing HA enriched in complex cyclic or branched structures, extended chains, diverse N-functional groups (e.g., heterocycles), and more oxidative moieties such as carboxyl, aldehyde, and ketone groups. Compared with removed HA ($H/C = 1.119$, $O/C = 0.429$), newly formed HA ($H/C = 1.064$, $O/C = 0.447$) was more unsaturated, aromatic, and oxidized. Consistent with KMD analysis (Figs. 3e, 4), large condensed aromatics in original HA were partially degraded, while exogenous inputs generated smaller carbon structures that underwent oxidation, dehydrogenation, and aromatization to form new HA components.

Across these complementary analyses, the results suggest that these functional-group and molecular features suggest distinct structural implications at the soil level. Oxygen-rich moieties may favor mineral-surface adsorption, particle bridging, and the initial formation of microaggregate-associated organic matter, whereas aromatic and condensed structures may favor compact aggregate interiors and greater resistance to structural disruption. Accordingly, the co-application likely promotes both interfacial anchoring and internal reinforcement of soil organic assemblies, making it potentially more favorable for the formation and persistence of organo mineral associated microaggregates.

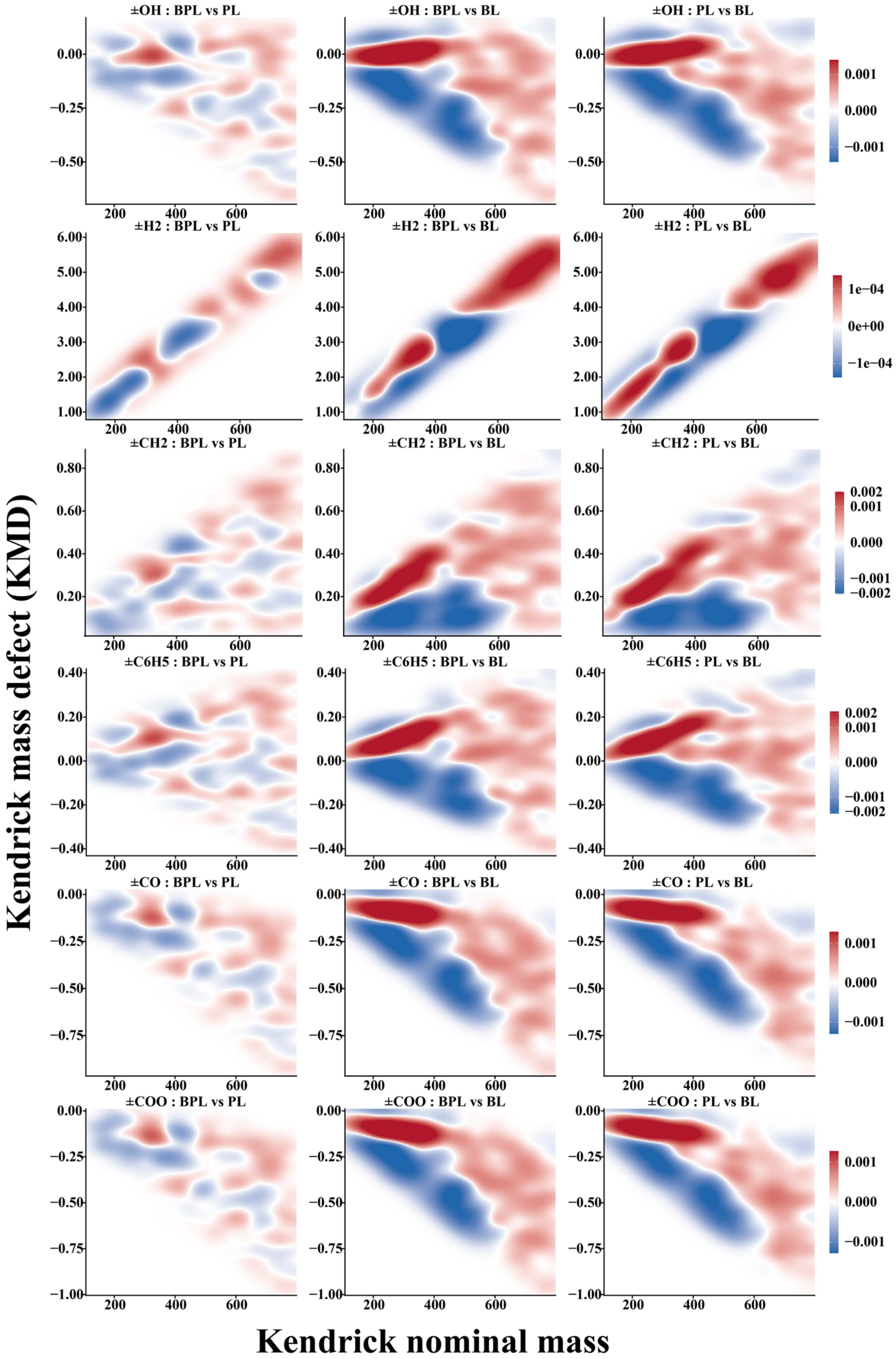

Fig. 4 Density difference maps of Kendrick mass defect (KMD) distributions for six homologous reaction series (±CH_2, ±COO, ±H_2, ±OH, ±C_6H_5, and ±CO) across different treatments. For each reaction series, pairwise comparisons between treatments (BPL vs PL, BPL vs BL, and PL vs BL) are shown as two-dimensional kernel density estimation (KDE) difference maps in Kendrick nominal mass-KMD space. Color intensity represents the difference in point density between the two treatments, with red indicating regions enriched in the first treatment and blue indicating regions enriched in the second treatment. Density differences were calculated using identical KNM and KMD ranges for each reaction series to ensure comparability. All panels share a common color scale within each reaction series. Across the six homologous series, PL showed relatively greater density in low to intermediate KNM regions for oxygen-related and hydrogenation-associated series (±OH, ±CO, ±COO, and ±H_2), whereas BL showed greater density in higher KNM regions for alkyl- and aromatic-related series (±CH_2 and ±C_6H_5). BPL showed an intermediate but broader redistribution

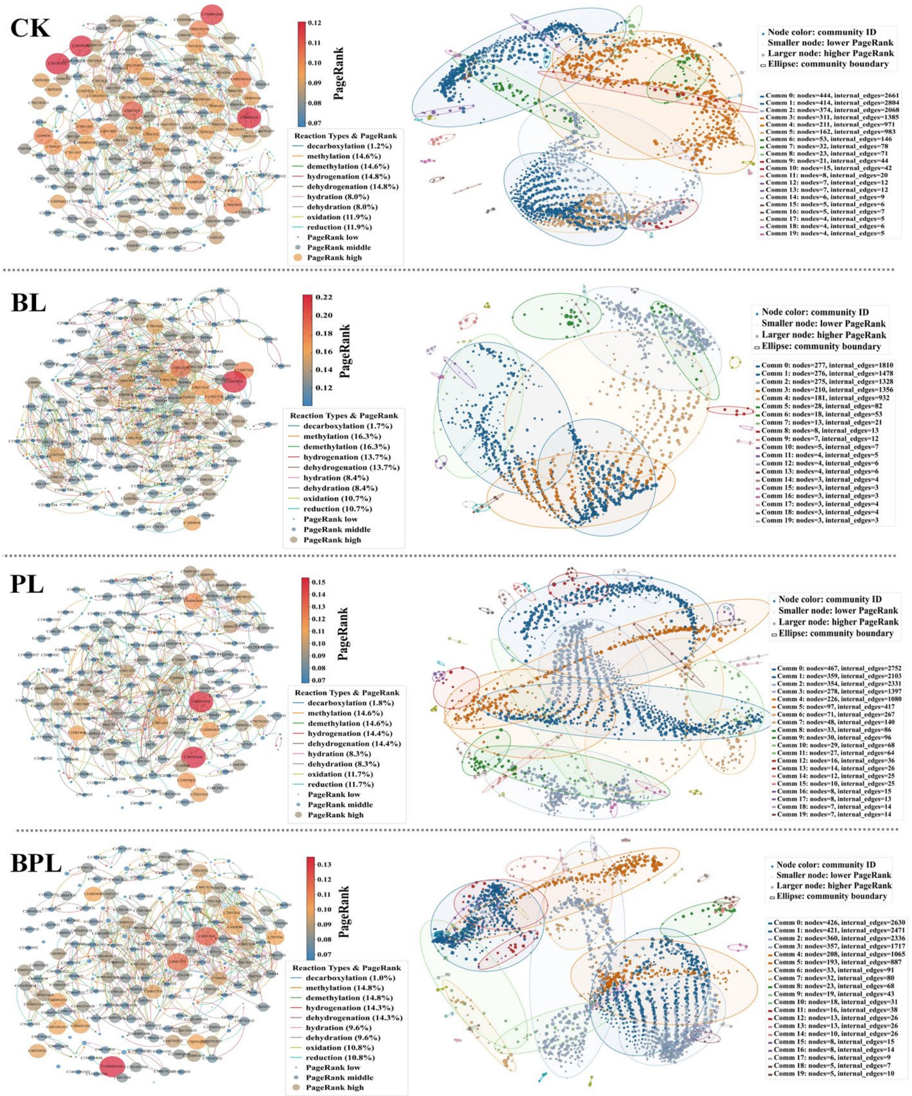

Fig. 5 Network organization and modular structure of humic acid (HA) molecular assemblages under different treatments. Directed molecular reaction networks were constructed from FT-ICR-MS assigned molecular formulas based on mass difference inferred transformations. Node size is proportional to PageRank values, with larger nodes representing higher PageRank scores, and node color denoting community membership. And node color denotes community membership. Ellipses outline major molecular communities identified by modularity based community detection

3.4 Network-based analysis highlights distinct molecular organization patterns and inferred transformation spaces

Directed molecular reaction networks were constructed based on FT-ICR-MS assigned molecular formulas to explore how different exogenous carbon inputs were associated with the organization and connectivity of HA molecular assemblages (Fig. 5 and Table S4). Rather than representing directly observed biogeochemical reaction sequences, these networks describe putative transformation relationships inferred from exact mass differences corresponding to common biochemical reactions. Differences among treatments were therefore interpreted in terms of network organization, molecular connectivity, and the relative prominence of inferred transformation types, providing a framework to compare how straw, biochar, and their combined application influence the potential transformation space of HA molecules (Simpson et al. 2002; Lehmann et al. 2011; Kleber et al. 2015). In the straw application (PL), network cores were dominated by low molecular weight, nitrogen containing HA associated components. Their PageRank scores were positively related to molecular abundance but negatively correlated with molecular mass, suggesting that network importance was concentrated in relatively low molecular weight, nitrogen-containing HA components that are commonly considered more chemically reactive (Simpson et al. 2002; Hertkorn et al. 2008; Lehmann and Kleber 2015). Although straw application substantially increased molecular diversity and overall network size, the high PageRank subnetwork exhibited low connectivity, with newly introduced molecules largely remaining peripheral rather than integrating into a coherent core structure. This pattern suggests that straw application primarily increases molecular diversity and network size, while the highly connected core structure remains relatively dispersed, indicating limited reorganization of network connectivity (Lehmann et al. 2011; Kleber et al. 2015). In contrast, biochar application (BL) was associated with increased core connectivity and a shift of high PageRank nodes toward higher molecular weight and more hydrophobic HA components, substantially weakening the negative relationship between PageRank and molecular mass (Simpson et al. 2002; Schmidt et al. 2011b; Cai et al. 2022; Cheng et al. 2024). Within the BL core network, transformations involving ± CH_2 mass differences accounted for a larger share of inferred links, whereas redox and decarboxylation related mass differences occurred less often. The network was weighted toward carbon-skeleton modification rather than redox or decarboxylation relationships (Schmidt et al. 2011b; Kleber et al. 2015; Jin et al. 2018; Chae et al. 2024). Co-application (BPL) preserved a large network and strong core connectivity. The core contained low molecular weight HA components and moderately unsaturated mid range molecules, with ± CH_2, ± H_2, and ± H_2O mass difference relationships co-occurring within the network. This core placed low-molecular-weight reactive components and structurally complex HA molecules in central positions (Newman 2006; Kleber et al. 2015; Cheng et al. 2024).

Community level reaction types sharpened these contrasts at the modular scale (Fig. 5; Tables S5–S8). The HA networks in PL comprised 854 communities with mixed reaction types and weak functional specialization, numerous parallel molecular associations rather than a few highly specialized modules(Hertkorn et al. 2008; Barabási Sciences 2013; Che et al. 2021). By contrast, the BL network contained 310 communities, with larger average module size and pronounced enrichment of ± CH_2 (methylation/demethylation) and ± H_2 reactions, accompanied by a relative depletion of decarboxylation processes (Lehmann et al. 2011; Kleber et al. 2015). ± CH_2 dominated transformations and lower modularity, BL thus favors conservative molecular transformation pathways, that preserved carbon backbones through stepwise methylation and demethylation (Schmidt et al. 2011b; Underwood et al. 2024). The BPL treatment had an intermediate modular pattern with higher complexity: community count approached PL; several mid to large communities showed co-enrichment of ± CH_2, ± H_2, and ± H_2O reactions, co-application maintained high reaction diversity and promoted biochar driven modular core formation, thereby facilitating the integration of straw derived reactive components into HA functional modules with well defined mechanistic signatures (Kleber et al. 2015; Sun et al. 2022; Cao et al. 2023; Li et al. 2025b).

Centrality analysis further clarified the roles of key molecular (Fig. 6). Under PL, low molecular weight, nitrogen rich HA components showed high local connectivity and global influence, low molecular weight HA components occupied central positions in loosely coupled modules linked by intermediate sized HA molecules (Lu et al. 2024; Zhou et al. 2024). BL shift this network hierarchy, high betweenness centrality was concentrated in mid to high molecular weight O_4-class HA compounds linking multiple modules. Small HA components maintained high eigenvector centrality in densely connected cores. The split between structural bridge nodes and reactive core nodes increased structural organization within the HA molecular assemblage rather than purely kinetic control (Li et al. 2024; Zhang et al. 2024). Co-application (BPL) reinforced this role hierarchy. Straw associated molecular components occupied more central positions within the network in the presence of biochar associated mid to high molecular weight molecules (Zhang et al. 2024; Xie et al. 2025).

Extraction of highly connected molecular chains from the weighted network core was used to summarize dominant patterns of molecular connectivity under different treatments (Fig. 7 and Tables S9–12) (Cai et al. 2022; Gong et al. 2023). Under BL, only one representative reaction backbone was retained, comprising 26 nodes and 25 edges. This reaction chain shows a transformation from smaller to larger molecules and from oxygen-rich to oxygen-poor compositions, accompanied by increased unsaturation and enhanced aromatization, and also exhibits distinct stage-specific characteristics. Stage A ($C_8H_5O_5 \rightarrow C_{11}H_{13}O_5$), consecutive methylation and hydrogenation reactions dominate, leading to continuous expansion of the carbon skeleton and a transient increase in saturation during the early phase. Stage B ($C_{11}H_{13}O_5 \rightarrow C_{13}H_{11}O_3$) is characterized mainly by dehydration, dehydrogenation, and formal reduction, with intermittent hydration and methylation steps, resulting overall in the loss of oxygen-containing functional groups and increased conjugation. In Stage C

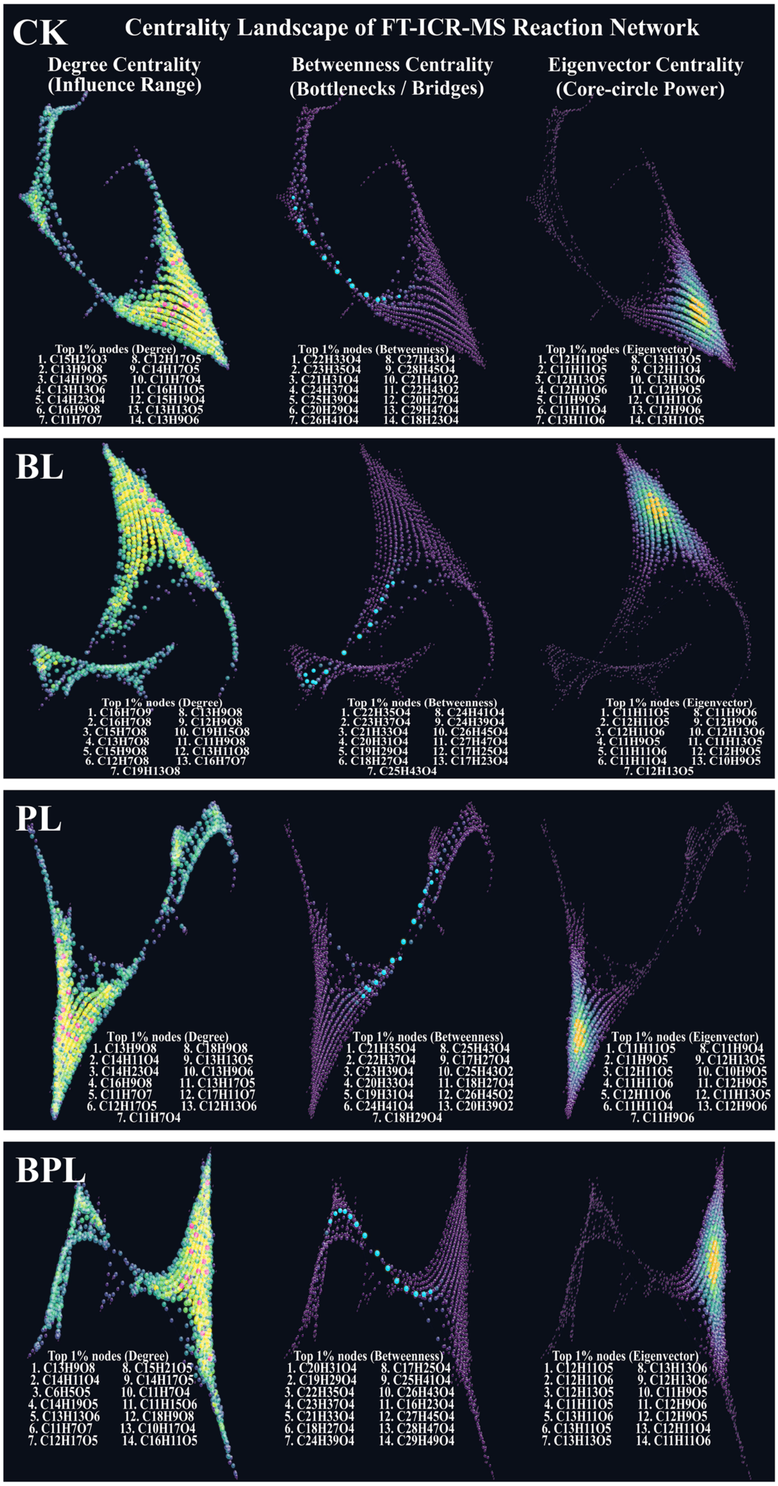

Fig. 6 Centrality landscape of HA molecular reaction networks under different treatments. The centrality landscape illustrates the distribution of degree, betweenness, and eigenvector centrality across molecular formulas, highlighting their distinct functional roles within the inferred reaction networks. Degree centrality represents local molecular connectivity, betweenness centrality identifies structural bridge molecules linking network modules, and eigenvector centrality indicates molecular formulas embedded within highly connected core regions

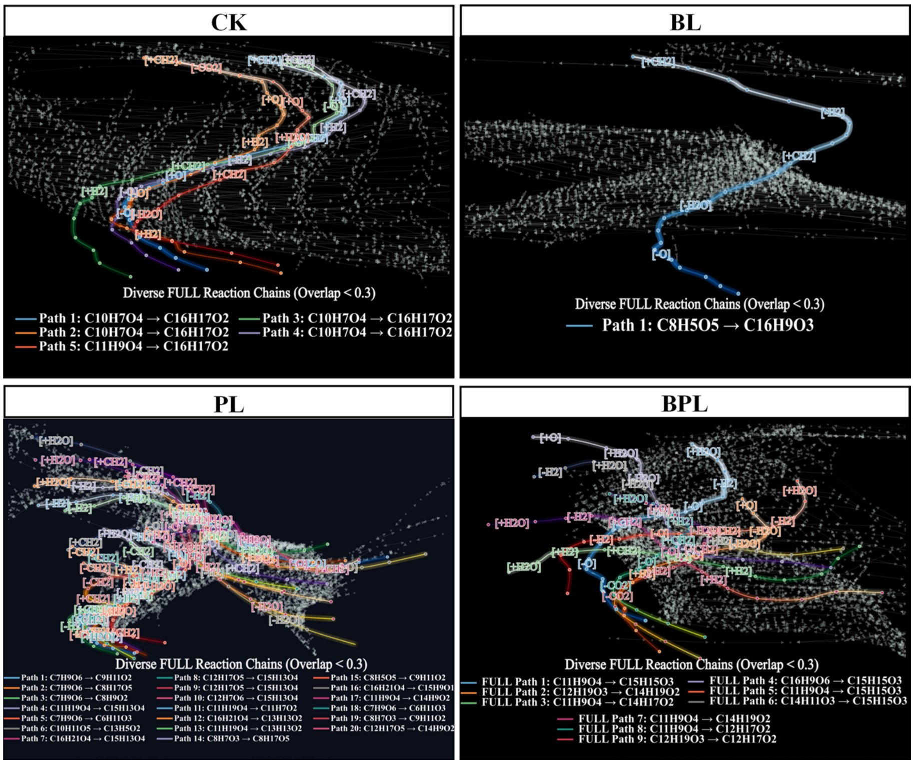

Fig. 7 Inferred reaction backbone chain detection of HA molecular reaction networks under different treatments. Inferred reaction backbone chains summarize dominant pathways of molecular connectivity extracted from the weighted networks, providing a complementary view of network organization and integration under different treatments

($C_{13}H_{11}O_3 \rightarrow C_{15}H_{11}O$), further methylation, dehydrogenation, and deoxygenation reactions occur, yielding progressively oxygen-depleted molecules; notably, $C_{15}H_{11}O_1$ represents the lowest-oxygen intermediate along this pathway. In Stage D ($C_{15}H_{11}O \rightarrow C_{16}H_{11}O_3 \rightarrow C_{16}H_9O_3$), a carboxylation step causes a local increase in oxygen content, followed by further dehydrogenation to generate the terminal highly unsaturated product. After biochar application, HA undergoes a continuous transformation jointly driven by methylation and dehydrogenation, involving carbon-skeleton expansion, a transient increase in saturation, deoxygenative condensation, terminal refunctionalization, and further dehydrogenation, ultimately leading to larger carbon skeletons, higher unsaturation, and enhanced aromatization.

Under PL treatment, 20 representative reaction pathways (D1–D20) were retained, with path lengths ranging from 11 to 15 nodes. The core HA molecular transformation network after straw application is composed of multiple medium-length pathways that are relatively independent but share several key intermediates. (1) In the low molecular weight region, multiple pathways originate from oxygen-rich precursors such as $C_7H_9O_6$, $C_8H_7O_3$, and $C_8H_5O_5$. Through demethylation, dehydration, reduction, and hydrogenation, these pathways repeatedly converge on intermediates such as $C_6H_5O_3$, $C_6H_7O_3$, $C_6H_9O_3$, and $C_7H_{11}O_3$, and then diverge further. One branch continues through deoxygenation and renewed methylation, ultimately forming low oxygen products such as $C_8H_9O_2$ and $C_9H_{11}O_2$. The other forms a stabilization branch, in which hydration and hydrogenation lead to relatively hydrogen-rich and oxygen-rich products such as $C_8H_{17}O_5$ and $C_6H_{11}O_3$. (2) In the medium and high molecular weight region, the pathways generally proceed through three stages: initial unsaturation increase and side chain adjustment, followed by deoxygenation and skeleton transformation, and finally the formation of low oxygen, highly unsaturated products. Starting from precursor molecules such as $C_{11}H_{19}O_4$, $C_{12}H_{17}O_5$, and $C_{16}H_{21}O_4$, these pathways undergo successive dehydrogenation, dehydration, methylation/demethylation, and reduction, and gradually converge on low oxygen, highly unsaturated products such as $C_{13}H_{13}O_2$, $C_{15}H_{13}O_4$, $C_{15}H_9O1$, and $C_{14}H_9O_2$.

In BPL, HA molecular transformation is characterized by initial activation through oxidation and hydration, followed by dehydration, reduction, decarboxylation, methylation, and hydrogenation, ultimately converging on a limited number of low oxygen, more highly hydrogenated, or re-alkylated products. The molecular transformation network can be broadly divided into two major trajectories. (1) The convergence of aromatic oxygen-containing precursors toward relatively low-oxygen, more highly hydrogenated C15 products. These pathways start from relatively unsaturated oxygenated molecules such as $C_{11}H_9O_4$, $C_{16}H_9O_6$, and $C_{14}H_{11}O_3$, which first undergo hydration, oxidation, or related activation steps to form more oxygenated intermediates (e.g. $C_{11}H_9O_4$-$C_{11}H_{11}O_5$, $C_{16}H_9O_6$-$C_{16}H_9O_7$, $C_{14}H_9O_3$-$C_{15}H_9O_5$). The pathways then repeatedly pass through nodes such as C14H9O6, $C_{14}H_{11}O_4$, and $C_{15}H_{13}O_4$, and ultimately converge on $C_{15}H_{15}O_3$. (2) The conversion of moderately oxidized intermediates into low oxygen, highly hydrogenated products such as $C_{14}H_{19}O_2$ and $C_{12}H_{17}O_2$. These pathways mainly originate from $C_{12}H_{19}O_3$ or from intermediates formed through early reduction and hydrogenation, then proceed through oxidation or hydration, followed by dehydration, dehydrogenation, reduction, and successive hydrogenation, ultimately yielding products such as $C_{14}H_{19}O_2$, $C_{14}H_{17}O_2$, and $C_{12}H_{17}O_2$.

In contrast to the single-application (BL, PL), HA transformation under BPL follows a sequence of initial activation, structural transformation, and final deoxygenation with pathway convergence. In the early stage, oxidation and hydration act as activation steps, increasing oxygen content or altering functional-group states. In the middle stage, methylation, dehydrogenation, dehydration, and reduction restructure the carbon skeleton and modify the degree of unsaturation. In the late stage, decarboxylation, reduction, and successive hydrogenation lead to terminal products with lower oxygen content, higher hydrogenation, or renewed alkylation. Compared with BL and PL, BPL shows several distinctive features: (1) Oxidation and hydration occur earlier and more concentratively. Rather than undergoing direct deoxygenation, some precursor molecules first form more highly oxygenated intermediates through oxygen addition or hydration before entering subsequent transformation steps. (2) Dehydrogenation is concentrated mainly in the early to middle stages and is often coupled with methylation and dehydration, whereas hydrogenation occurs more frequently in the middle to late stages and is commonly associated with reduction and decarboxylation. The network therefore follows a pattern of increasing unsaturation followed by partial re-hydrogenation. (3) Consecutive methylation along multiple pathways reflects not only changes in oxygen-containing functional groups but also side-chain growth and substituent reorganization. (4) Carboxylation occurs mainly in the middle stage and redirects relatively low-oxygen intermediates toward more oxygenated nodes, whereas decarboxylation in the later stage lowers oxygen content and promotes pathway convergence, followed by successive hydrogenation that produces more stable low oxygen end products.

By integrating the representative reaction chains of the different treatments, BL, PL and BPL, it can be found that although the exogenous carbon input methods are different, the intermediate molecules involved in the HA molecular transformation process are still mainly concentrated within a relatively fixed molecular range. $C_{13}H_{15}O_4$, $C1_3H_{15}O_3$, and $C_{15}H_{13}O_4$ repeatedly appear in the transformation and convergence stages of the later portions of reaction chains across treatments, linking multiple transformation steps, including dehydrogenation, reduction, dehydration, methylation, carboxylation/decarboxylation, and hydrogenation. These molecules may function as key reaction hubs and require further validation.

In the BL main chain, $C_{11}H_{13}O_5$, $C_{13}H_{13}O_5$, and $C_{15}H_{11}O$ act as key intermediates at critical junctions, corresponding to early-stage chain elongation, mid stage transformation, and late stage deoxygenation, linking two distinct reaction types. In PL, the low molecular weight compounds $C_6H_5O_3$, $C_6H_7O_3$, $C_6H_9O_3$, and $C_7H_{11}O_3$ recur across multiple pathways and likely act as important intermediates in the conversion of oxygen-rich small molecules toward deoxygenation branches or hydration/hydrogenation branches. In the medium to high molecular weight region, $C_{14}H_{15}O_3$, $C_{15}H_{15}O_5$, and $C_{15}H_{13}O_4$ repeatedly occur in the later stages of the reaction network and may serve as key convergence nodes during humification after straw addition. In the BPL treatment, $C_{11}H_{11}O_5$, $C_{14}H_9O_6$, and $C_{15}H_9O_5$ are mainly associated with intermediates formed during the early activation stage through oxidation, hydration, or carboxylation, whereas $C_{14}H_{11}O_5$, $C_{14}H_{11}O_4$, $C_{14}H_{15}O_3$, and $C_{15}H_{15}O_5$ are concentrated in the middle and late stages, where transformation and convergence dominate. Based on the above analyses, we infer that the HA molecular transformation network may not be a disordered heterogeneous system composed of numerous discrete molecules or an unstructured molecular continuum, but instead an organized network in which a small number of core intermediates act as key transformation hubs and different classes of molecular clusters participate in stepwise modification and coordinated transformation.

These network patterns further support that co-application did not simply mix two independent carbon inputs, but reorganized straw-associated reactive intermediates within biochar-associated aromatic and structurally persistent molecular frameworks, mainly involving condensed aromatics, aromatic domains, and quinone-/phenolic-containing moieties. It should be emphasized that the molecular reaction networks constructed in this study are based on exact mass differences and predefined reaction rules, and therefore represent inferred transformation relationships rather than directly observed biogeochemical reactions. While these networks provide valuable insights into molecular organization, connectivity, and potential transformation spaces of HA, they do not imply that all inferred reactions occur sequentially or at comparable rates in situ. Accordingly, interpretations are framed in terms of network structure and association rather than explicit reaction mechanisms.

4 Conclusion

Co-application of straw and biochar produced a distinct interaction effect during humic acid formation. Straw favored oxygen-rich and chemically accessible components, whereas biochar enriched aromatic and structurally condensed domains. Under co-application, straw-derived reactive intermediates were retained within biochar-associated aromatic domains and incorporated into HA that combined high oxygenation, elevated radical activity, and persistent aromatic features.

These changes was expressed not simply as a change in bulk composition, co-application shifted the aromatic pool away from highly condensed domains toward less condensed yet still aromatic forms, while bringing low molecular weight reactive components into closer association with structurally complex molecules in the transformation network. The dominant outcome was therefore not additive carbon accumulation, but the coexistence of chemically distinct components within the same HA system.

Under co-application, HA retained oxygen-rich and radical-active components alongside aromatic and structurally condensed domains, a pattern here termed reactivity-stability coupling. In this context, stabilization potential may depends not only on intrinsically recalcitrant molecules, but also on the retention of reactive components within persistent aromatic environments. This provides a more precise basis for interpreting how mixed organic inputs regulate soil carbon stabilization.

Supplementary Information

The online version contains supplementary material available at https://doi.org/10.1007/s42773-026-00622-y.

Supplementary material 1. The Supplementary Information provides a detailed record of the systematic analyses and methodological procedures used to assess how straw and mature biochar influence the molecular conformation and reactivity of soil humic acid (HA). Experimental methods documented include elemental analysis, fluorescence excitation-emission matrix (EEM) spectroscopy and derived indices (HIX, FI, BIX), transmission electron microscopy (TEM), electron paramagnetic resonance (EPR), solid-state ^{13}C nuclear magnetic resonance (13C NMR), and the processing of high-resolution electrospray ionization Fourier transform ion cyclotron resonance mass spectrometry (FT-ICR-MS) data, together with FT-ICR-MS based construction and analysis of molecular-transformation networks. In addition to methodological descriptions, the Supporting Information contains supporting datasets and statistical details: basic physicochemical properties of straw and biochar; characterization of HA acidic functional sites; the description and calculation of spectroscopic parameters used for HA characterization; molecular-network data for each treatment (nodes, edges, and counts of reaction types); and information on reaction communities of all types with internal edges > 2 across treatments; Detailed information on the top 20 non-redundant primary reaction chains extracted from each treatment by applying the path overlap constraint (overlap < 0.3).

Author contributions

Rui Ma: analyzed the data and wrote the article. Zhenging Shi and Yifeng-Zhang: revised the manuscript. Yifeng Zhang, Wenke Zhang, Xiaodong Zheng, Xiang Li, LanWei, Lianxi Huang: collected experimental soil samples and conducted all experiments. Qimei Lin: designed the whole experiment and revised the manuscript. Zhongzhen Liu: designed the whole experiment and submitted the manuscript. The first draft of the manuscript was written by Rui Ma and all authors commented on previous versions of the manuscript. All authors read and approved the final manuscript.

Funding

This work was supported by the National Natural Science Foundation of China (42207316), the Postdoctoral Fellowship Program of CPSF, China (No. GZC20232641), and the China Postdoctoral Science Foundation (No. 2024M753215) and Low carbon agriculture and carbon neutralization Research Center, GDAAS (XT202220).

Data availability

The datasets used or analyzed during the current study are available from the corresponding author upon reasonable request.

Declarations

Competing interests

Qimei Lin is an EBM of the journal Biochar, and he was not involved in the peer-review or handling of the manuscript. The authors declare no competing financial interest.

Author details

[1]Key Laboratory of Plant Nutrition and Fertilizer in South Region, Ministry of Agriculture, Guangdong Key Laboratory of Nutrient Cycling and Farmland Conservation, Institute of Agricultural Resources and Environment, Guangdong Academy of Agricultural Sciences, Guangzhou 510640, Guangdong, China. [2]State Key Laboratory of Black Soils Conservation and Utilization, Northeast Institute of Geography and Agroecology, Chinese Academy of Sciences, Changchun 130102, Jilin, China. [3]Key Laboratory of Pollution Control and Ecosystem Restoration in Industry Clusters, Ministry of Education, School of Environment and Energy, South China University of Technology, Guangzhou 510006, Guangdong, China.

Received: 18 January 2026 Revised: 25 March 2026 Accepted: 13 April 2026

Published online: 03 June 2026

References

Ateia M, Ran J, Fujii M, Yoshimura C (2017) The relationship between molecular composition and fluorescence properties of humic substances. Int J Environ Sci Technol 14:867–880

Barabási A-L (2013) Network science. Phys Sci 371:20120375

Baveye PC, Wander M (2019) The (bio)chemistry of soil humus and humic substances: why is the "new view" still considered novel after more than 80 years? Front Environ Sci 2019(7):27

Bi D, Huang F, Jiang M, He Z, Lin X (2022) Effect of pyrolysis conditions on environmentally persistent free radicals (EPFRs) in biochar from co-pyrolysis of urea and cellulose. Sci Total Environ 805:150339

Bonacich P (1987) Power and centrality: a family of measures. J a J O S 92:1170–1182

Brandes U (2001) A faster algorithm for betweenness centrality. J t J O m s 25:163–177

Brin S, Page L (1998) The anatomy of a large-scale hypertextual Web search engine. Comput Networks ISDN Syst 30:107–117

Cai S, Liu M, Zhang Y, Hu A, Zhang W, Wang D (2022) Molecular transformation of dissolved organic matter and formation pathway of humic substances in dredged sludge under aerobic composting. Bioresource Technol 364:128141

Cai S, Zhang Y, Hu A, Liu M, Wu H, Wang D, Zhang W (2023) Dissolved organic matter transformation mechanisms and process optimization of wastewater sludge hydrothermal humification treatment for producing plant biostimulants. Water Res 235:119910

Cao Z, Deng F, Wang R, Li J, Liu X, Li D (2023) Bioaugmentation on humification during co-composting of corn straw and biogas slurry. Bioresource Technol 374:128756

Chae HG, Margenot AJ, Jeon J-R, Kim MS, Jang K-S, Yoon HY, Kim PJ, Lee JG (2024) Linking the humification of organic amendments with size aggregate distribution: insights into molecular composition using FT-ICR-MS. Sci Total Environ 927:172147

Che J, Bai Y, Li X, Ye J, Liao H, Cui P, Yu Z, Zhou S (2021) Linking microbial community structure with molecular composition of dissolved organic matter during an industrial-scale composting. J Hazard Mater 405:124281

Chen D, Xu J, Ling P, Fang Z, Ren Q, Xu K, Jiang L, Wang Y, Su S, Hu S, Xiang J (2024) Formation and evolution mechanism of persistent free radicals in biochar during biomass pyrolysis: insights from biochar's element composition and chemical structure. Fuel 357:129910

Cheng Z, Li A, Wang R, Hu Q, Zhou J, Li M, Wang T, He D, Zhu L (2024) Long-term straw return promotes accumulation of stable soil dissolved organic matter by driving molecular-level activity and diversity. Agric Ecosyst Environ 374:109155

Chin Y-P, Aiken G, O'Loughlin E (1994) Molecular weight, polydispersity, and spectroscopic properties of aquatic humic substances. Environ Sci Technol 28:1853–1858

Cory RM, McKnight DM (2005) Fluorescence spectroscopy reveals ubiquitous presence of oxidized and reduced quinones in dissolved organic matter. Environ Sci Technol 39:8142–8149

Cui S, Liu L, Zhang F, Fu Q, Ma C, Ding Y (2025) Compositional evolution of dissolved organic matter mobilized by straw incorporation and its climate-driven interactions with lead in cold-region black soil: decoding mechanisms through PARAFAC and complexation modeling. Carbon Res 4:56

de Aguiar TC, de Oliveira Torchia DF, van Tol de Castro TA, Tavares OCH, de Abreu Lopes S, de Souza da Silva L, Castro RN, Berbara RLL, Pereira MG, García AC (2022) Spectroscopic–chemometric modeling of 80 humic acids confirms the structural pattern identity of humified organic matter despite different formation environments. Sci Total Environ 833:155133

De Nobili M, Bravo C, Chen Y (2020) The spontaneous secondary synthesis of soil organic matter components: a critical examination of the soil continuum model theory. Appl Soil Ecol 154:103655

Di Gerónimo PF, Wyngaard N, Videla CdC (2026) Do residue quality and tillage systems modify nitrogen partitioning into different soil organic matter fractions? Soil Tillage Res 257:106944

Dou S, Zhang Y, Shan J, Wu M, Ma R, Guan S, Jia Z (2025) Soil organic matter revisited: why humic substances still matter. Pedosphere 36(1):6–11

Du Z, Sun Z, Li X, Zhou H, Shen F, Hou J, Dai L (2025) Unleashing redox activity of biochar via a green thermal air oxidation process: insights from machine learning. J Clean Prod 527:146718

Enebe MC, Ray RL, Griffin RW (2025) The impacts of biochar on carbon sequestration, soil processes, and microbial communities: a review. Biochar 7:107

Fedotov GN, Shein EV, Ushkova DA, Salimgareeva OA, Gorepekin IV, Potapov DI (2023) Supramolecular formations of humic substance molecules and their fractal organization. Eurasian Soil Sci 56:1007–1013

Freeman LC (1978) Centrality in social networks conceptual clarification. Soc Netw 1:215–239

Fu Y, Xu Y, Wang Q, Van Zwieten L, Liang C, Xu J, Guggenberger G, Luo Y (2025) Deciphering the microbial players driving straw decomposition and accumulation in soil components of particulate and mineral-associated organic matter. Soil Biol Biochem 209:109871

Gong X, Zou L, Wang L, Zhang B, Jiang J (2023) Biochar improves compost humification, maturity and mitigates nitrogen loss during the vermicomposting of cattle manure-maize straw. J Environ Manage 325:116432

Goranov AI, Tadini AM, Martin-Neto L, Bernardi AC, Oliveira PP, Pezzopane JR, Milori DM, Mounier S, Hatcher PG (2022) Comparison of sample preparation techniques for the (−) ESI-FT-ICR-MS analysis of humic and fulvic acids. Environ Sci Technol 56:12688–12701

Guo S, Zou Z, Chen Y, Long X, Liu M, Li X, Tan J, Chen R (2023) Synergistic effect of hydrogen bonding and π-π interaction for enhanced adsorption of rhodamine B from water using corn straw biochar. Environ Pollut 320:121060

Hagberg A, Swart PJ, Schult DA. Exploring network structure, dynamics, and function using NetworkX. In. Los Alamos National Laboratory (LANL). 2007.

Han L, Hu A, Mzuka HL, Chen X, Shen J, Wang J (2025) Molecular properties of dissolved organic matter across Earth systems: a meta-analysis. J Earth Sci 36:2674–2688

Hayes MH, Clapp CE (2001) Humic substances: considerations of compositions, aspects of structure, and environmental influences. Soil Sci 166:723–737

He D, Yang R, Fu Y, Zhu B (2025) Superior properties of biochar contribute to soil carbon sequestration and climate change mitigation. J Environ Chem Eng 13:116936

Helal AA, Murad GA, Helal AA (2011) Characterization of different humic materials by various analytical techniques. Arab J Chem 4:51–54

Hertkorn N, Frommberger M, Witt M, Koch BP, Schmitt-Kopplin P, Perdue EM (2008) Natural organic matter and the event horizon of mass spectrometry. Anal Chem 80:8908–8919

Hughey CA, Hendrickson CL, Rodgers RP, Marshall AG, Qian K (2001) Kendrick mass defect spectrum: a compact visual analysis for ultrahigh-resolution broadband mass spectra. Anal Chem 73:4676–4681

Jia H, Zhao S, Shi Y, Zhu L, Wang C, Sharma VK (2018) Transformation of polycyclic aromatic hydrocarbons and formation of environmentally persistent free radicals on modified montmorillonite: the role of surface metal ions and polycyclic aromatic hydrocarbon molecular properties. Environ Sci Technol 52:5725–5733

Jia P, Wang X, Liu S, Hua Y, Zhou S, Jiang Z (2023) Combined use of biochar and microbial agent can promote lignocellulose degradation and humic acid formation during sewage sludge-reed straw composting. Bioresource Technol 370:128525

Jin J, Sun K, Yang Y, Wang Z, Han L, Wang X, Wu F, Xing B (2018) Comparison between soil- and biochar-derived humic acids: composition, conformation, and phenanthrene sorption. Environ Sci Technol 52:1880–1888

Jindo K, Sonoki T, Matsumoto K, Canellas L, Roig A, Sanchez-Monedero MA (2016) Influence of biochar addition on the humic substances of composting manures. Waste Manag 49:545–552

Kellerman AM, Guillemette F, Podgorski DC, Aiken GR, Butler KD, Spencer RGM (2018) Unifying concepts linking dissolved organic matter composition to persistence in aquatic ecosystems. Environ Sci Technol 52:2538–2548

Kitson E, Kew W, Ding W, Bell NGA (2021) PyKrev: a Python library for the analysis of complex mixture FT-MS data. J Am Soc Mass Spectrom 32:1263–1267

Kleber M, Eusterhues K, Keiluweit M, Mikutta C, Mikutta R, Nico PS (2015) Chapter one - mineral-organic associations: formation, properties, and relevance in soil environments. In: Sparks DL (ed) Advances in Agronomy. Academic Press, pp 1–140

Koyama T, Enggrob KL, Rasmussen J, Martins JT, Peixoto L (2025) Substrate quantity and quality affect microbial carbon use efficiency and priming effects of root exudates investigated with microdialysis. Soil Biol Biochem 209:109869

Lehmann J, Kleber M (2015) The contentious nature of soil organic matter. Nature 528:60–68

Lehmann J, Rillig MC, Thies J, Masiello CA, Hockaday WC, Crowley D (2011) Biochar effects on soil biota – a review. Soil Biol Biochem 43:1812–1836

Lei K, Dai W, Wang J, Li Z, Cheng Y, Jiang Y, Yin W, Wang X, Song X, Tang Q (2024a) Biochar and straw amendments over a decade divergently alter soil organic carbon accumulation pathways. Agronomy 14:2176

Lei K, Dai W, Wang J, Li Z, Cheng Y, Jiang Y, Yin W, Wang X, Song X, Tang Q (2024b) Biochar and straw amendments over a decade divergently alter soil organic carbon accumulation pathways. Agronomy. https://doi.org/10.3390/agronomy14092176

Li S, He P, Zhang H, Shao L, Lü F (2024) Variations in redox properties of biochar and humic acid induced by interactive molecular exchange. Carbon Res 3:26

Li H, Duan W, Jiang H, Zhang M, Lang D, Du W, Chang Z, Zhang P, Pan B (2025a) Formation of environmentally persistent free radicals on molecular sieves: the role of Lewis acid sites. Ecotoxicol Environ Saf 304:119121

Li M, Jiang H, Li R, Liu W, Xie Y, Wu W, Liu D, Wu M, Qiu Z (2025b) Effects of biochar-loaded microbial agent in regulating nitrogen transformation and integration into humification for straw composting. Bioresource Technol 417:131873

Liang Z, Rasmussen J, Poeplau C, Elsgaard L (2023) Priming effects decrease with the quantity of cover crop residues – potential implications for soil carbon sequestration. Soil Biol Biochem 184:109110

Liu Z, Wu X, Liu W, Bian R, Ge T, Zhang W, Zheng J, Drosos M, Liu X, Zhang X, Cheng K, Li L, Pan G (2020) Greater microbial carbon use efficiency and carbon sequestration in soils: amendment of biochar versus crop straws. GCB Bioenergy 12:1092–1103

Liu H-t, Guo H-n, Guo X-x, Wu S (2021) Probing changes in humus chemical characteristics in response to biochar addition and varying bulking agents during composting: a holistic multi-evidence-based approach. J Environ Manage 300:113736

Liu H, Wang X, Song X, Leng P, Li J, Mazza Rodrigues JL, Hong Z, Kuzyakov Y, Xu J, Dai Z (2022a) Generalists and specialists decomposing labile and aromatic biochar compounds and sequestering carbon in soil. Geoderma 428:116176

Liu X, An Q, Song X, Hussain Q, Cui L, Wang C, Wang Y, Cui D (2022b) Urease and β-glucosidase activity enhanced the transformation of functional groups of humin amended by straw and straw-derived biochar. Chem Biol Technol Agric 9:87

Liu X, Chen Z, Lu S, Shi X, Qu F, Cheng D, Wei W, Shon HK, Ni B-J (2024) Persistent free radicals on biochar for its catalytic capability: a review. Water Res 250:120999

Liu G, Hua J, Wei J, Yang L, Chen N, Fang G, Zhang S (2025) A critical review on the biochar-mediated formation of reactive species: detection methods, transformation mechanisms and environmental implications. Bull Environ Contam Toxicol 114:70

Lu M, Lin B, Zhang Y, Hao Y, Li K, Huang Z, Li J (2024) Insight into the molecular transformation pathways of humic acid in the co-composting of bagasse and cow manure after adding compound microorganisms. Process Biochem 143:23–33

Luo X, Dou S, Jia N, Guan S, Guo D, Zhang B, Yalihong D (2025) Alkali extracts (humus-like substances) of straw have higher chemical activity than those of straw-derived biochar. J Environ Chem Eng 13:115571

Meng W, Zhu F, Wang X, Guan S, Dou S, Ndzelu BS (2023) Contrasting effects of straw and straw-derived biochar application on soil organic matter and corn yield in a Chinese Mollisol. J Soils Sediments 23:3843–3856

Newman MEJ (2006) Modularity and community structure in networks. Proc Natl Acad Sci U S A 103:8577–8582

Odinga ES, Waigi MG, Gudda FO, Wang J, Yang B, Hu X, Li S, Gao Y (2020) Occurrence, formation, environmental fate and risks of environmentally persistent free radicals in biochars. Environ Int 134:105172

Ohno T, Parr TB, Gruselle MCI, Fernandez IJ, Sleighter RL, Hatcher PG (2014) Molecular composition and biodegradability of soil organic matter: a case study comparing two New England forest types. Environ Sci Technol 48:7229–7236

Olk DC, Bloom PR, Perdue EM, McKnight DM, Chen Y, Farenhorst A, Senesi N, Chin YP, Schmitt-Koplin P, Hertkorn N, Harir M (2019) Environmental and agricultural relevance of humic fractions extracted by alkali from soils and natural waters. J Environ Qual 48:1126–1126

Ou J, Wen J, Tan W, Luo X, Cai J, He X, Zhou L, Yuan Y (2023) A data-driven approach for understanding the structure dependence of redox activity in humic substances. Environ Res 219:115142

Page L, Brin S, Motwani R, Winograd T (1999a) The PageRank Citation Ranking: Bringing Order to the Web. In: The Web Conference.

Page L, Brin S, Motwani R, Winograd T (1999b) The PageRank citation ranking: Bringing order to the web. In., Stanford infolab.

Piccolo A (2001) The supramolecular structure of humic substances. Soil Sci 166:810–832

Piccolo A (2016) In memoriam Prof. F.J. Stevenson and the question of humic substances in soil. Chem Biol Technol Agric 3:23

Premalatha RP, Poorna Bindu J, Nivetha E, Malarvizhi P, Manorama K, Parameswari E, Davamani V (2023) A review on biochar's effect on soil properties and crop growth. Front Energy Res. 2023(11):1092637

Qin Y, Li G, Gao Y, Zhang L, Ok YS, An T (2018) Persistent free radicals in carbon-based materials on transformation of refractory organic contaminants (ROCs) in water: a critical review. Water Res 137:130–143

Rashid MS, Liu G, Yousaf B, Hamid Y, Rehman A, Arif M, Ahmed R, Ashraf A, Song Y (2022) A critical review on biochar-assisted free radicals mediated redox reactions influencing transformation of potentially toxic metals: occurrence, formation, and environmental applications. Environ Pollut 315:120335

Ruan X, Sun Y, Du W, Tang Y, Liu Q, Zhang Z, Doherty W, Frost RL, Qian G, Tsang DCW (2019) Formation, characteristics, and applications of environmentally persistent free radicals in biochars: a review. Bioresource Technol 281:457–468

Schmidt MW, Torn MS, Abiven S, Dittmar T, Guggenberger G, Janssens IA, Kleber M, Kögel-Knabner I, Lehmann J, Manning DAJN (2011a) Persistence of soil organic matter as an ecosystem property. Nature 478:49–56

Schmidt MWI, Torn MS, Abiven S, Dittmar T, Guggenberger G, Janssens IA, Kleber M, Kögel-Knabner I, Lehmann J, Manning DAC, Nannipieri P, Rasse DP, Weiner S, Trumbore SE (2011b) Persistence of soil organic matter as an ecosystem property. Nature 478:49–56

Shi Y, Dai Y, Liu Z, Nie X, Zhao S, Zhang C, Jia H (2020) Light-induced variation in environmentally persistent free radicals and the generation of reactive radical species in humic substances. Front Environ Sci Eng 14:106

Simpson AJ, Kingery WL, Hayes MH, Spraul M, Humpfer E, Dvortsak P, Kerssebaum R, Godejohann M, Hofmann M (2002) Molecular structures and associations of humic substances in the terrestrial environment. Naturwissenschaften 89:84–88

Stancampiano LM, Verrillo M, Cangemi S, Meignant I, Spaccini R, Piccolo A, Bridoux MC (2023) The molecular composition of humic substances extracted from green composts and their potential for soil remediation. Environ Chem Lett 21:2489–2498

Sun Q, Yang X, Meng J, Lan Y, Han X, Chen W, Huang Y (2022) Long-term effects of straw and straw-derived biochar on humic substances and aggregate-associated humic substances in brown earth soil. Front Environ Sci 2022(10):899935

Sutton R, Sposito G (2005) Molecular structure in soil humic substances: the new view. Environ Sci Technol 39:9009–9015

Swift RS (1996) Organic matter characterization. Methods Soil Anal Part Chem Methods. 5:1011–1069

Tao J, Liu X (2025) Identification of the key regulators of the soil carbon priming effect: a data synthesis. Plant Soil 514:555–569

Traquete F, Luz J, Cordeiro C, Sousa Silva M, Ferreira AEN (2022) Graph properties of mass-difference networks for profiling and discrimination in untargeted metabolomics. Front Mol Biosci 2022(9):917911

Trubetskaya OE, Selivanova OM, Rogachevsky VV, Trubetskoj OA (2023) Transmission electron microscopy of electrophoretic humic acids fractions obtained by coupling size exclusion chromatography-polyacrylamide gel electrophoresis: the next step to understanding structural organization of soil humic matter. Microchem J 193:109177

Trubetskaya OE, Selivanova OM, Rogachevskii VV, Trubetskoj OA (2024) Electron microscopy of stable electrophoretic fractions of natural humic acids as a key to the understanding of their structural organization. Russ J Bioorg Chem 50:766–777

Trubetskaya O, Selivanova O, Rogachevsky V, Trubetskoj O (2025) Transmission electron microscopy indicates supramolecular transformations over time of soil humic acids and their electrophoretic fractions. Chem Biol Technol Agric 12:143

Underwood TR, Bourg IC, Rosso KM (2024) Mineral-associated organic matter is heterogeneous and structured by hydrophobic, charged, and polar interactions. Proc Natl Acad Sci U S A 121:e2413216121

Wan Z, Sun Y, Tsang DCW, Khan E, Yip ACK, Ng YH, Rinklebe J, Ok YS (2020) Customised fabrication of nitrogen-doped biochar for environmental and energy applications. Chem Eng J 401:126136

Wang C, Tu Q, Dong D, Strong PJ, Wang H, Sun B, Wu W (2014) Spectroscopic evidence for biochar amendment promoting humic acid synthesis and intensifying humification during composting. J Hazard Mater 280:409–416

Wang J, Xiong Z, Kuzyakov Y (2016) Biochar stability in soil: meta-analysis of decomposition and priming effects. Gcb Bioenergy 8:512–523

Wiedner K, Rumpel C, Steiner C, Pozzi A, Maas R, Glaser B (2013) Chemical evaluation of chars produced by thermochemical conversion (gasification, pyrolysis and hydrothermal carbonization) of agro-industrial biomass on a commercial scale. Biomass Bioenergy 59:264–278

Xiao J, Shi Z, Liu F, Ye Q, Zhu L, Gao Q, Yang X, Tratnyek PG (2025) The molecular weight-dependent redox capacity of soil dissolved organic matter: roles of aromaticity and organic sulfur. Geochim Cosmochim Acta 401:174–189

Xie J, Latif J, Yang K, Wang Z, Zhu L, Yang H, Qin J, Ni Z, Jia H, Xin W, Li X (2024) A state-of-art review on the redox activity of persistent free radicals in biochar. Water Res 255:121516

Xie N, Fan Y, Duan N, Yang L, Radosevich M, Zhang Y, Wang Y, Wang J, Liang X (2025) Interactive effects of straw and biochar amendments on soil organic carbon stabilization and bacterial community dynamics. Biol Fertil Soils 61:1423–1437

Yang X, Yan R, Yang C, Zhang H, Lyu H, Li S, Liu T, Li R, Yao Y, Li W, Gao L (2024) Soil accelerates the humification involved in co-composting of wheat straw and cattle manure by promoting humus formation. Chem Eng J 479:147583

Yassine MM, Harir M, Dabek-Zlotorzynska E, Schmitt-Kopplin P (2014) Structural characterization of organic aerosol using fourier transform ion cyclotron resonance mass spectrometry: aromaticity equivalent approach. Rapid Commun Mass Spectrometr 28:2445–2454

Yi Y, Fu Y, Yang W, Chen W, Wang Y, Diao Z, Chen Z, Li Z (2025) Key role of π-π interactions for highly efficient removal of organic pollutants from water using boron-doped biochar. J Water Process Eng 69:106783

Ying J, Zhang X, Wu W, Nan Q, Wang G, Dong DJP (2024) The effects of long-term rice straw and biochar return on soil humus composition and structure in paddy soil. Plant Soil Environ 70:772–782

Zhang G, Dou S, Meng F, Yin X, Zhou X (2022) Transformation of biochar into extracted humic substances under short-term laboratory incubation conditions: evidence from stable carbon isotopes. Soil Tillage Res 215:105189

Zhang Z, Liu S, Wang X, Huang S, Sun K, Xia X (2023) Differences in structure and composition of soil humic substances and their binding for polycyclic aromatic hydrocarbons in different climatic zones. Environ Pollut 322:121121

Zhang J, Fan B, Zhao L, Zhao C, Yang F (2024) Biochar promotes compost humification by regulating bacterial and fungal communities. Front Microbiol 2024(15):1470930

Zhang Y, Dou S, Ma R, Ndzelu BS, Zhou J, Ren C, Xia Y, Wang K, Guan S (2025) Using 13C15N labeling technology to reveal the fate of maize straw in soil organic matter and dissolved organic matter under different exogenous microorganism-mediated conditions. J Agric Food Chem 73:21769–21785

Zhou Z, Fu Q-L, Fujii M, Waite TD (2023) Complementary elucidation of the molecular characteristics of groundwater dissolved organic matter using ultrahigh-resolution mass spectrometry coupled with negative- and positive-ion electrospray ionization. Environ Sci Technol 57:4690–4700

Zhou J, Gao W, Xie L, Zhang R, Zhang Y, Wei Z (2024) Revealing mechanism of phenol-amine reaction to form humus in compost based on high-resolution liquid chromatography mass spectrometry and spectroscopy. Bioresource Technol 403:130862